



Spatial and temporal trends in Precambrian nitrogen cycling: A Mesoproterozoic offshore nitrate minimum

Matthew C. Koehler^{a,*}, Eva E. Stüeken^{a,b,c}, Michael A. Kipp^a, Roger Buick^a,
Andrew H. Knoll^d

^a Department of Earth & Space Sciences and Astrobiology Program, University of Washington, Box 351310, Seattle, WA 98195, USA

^b Department of Earth Sciences, University of California, Riverside, CA 92521, USA

^c Department of Earth & Environmental Sciences, University of St Andrews, St Andrews KY16 9AL, Scotland, UK

^d Department of Organismic and Evolutionary Biology, Harvard University, Cambridge, MA 02138, USA

Received 6 August 2015; accepted in revised form 30 October 2016; available online 16 November 2016

Abstract

Fixed nitrogen is an essential nutrient for eukaryotes. As N₂ fixation and assimilation of nitrate are catalyzed by metalloenzymes, it has been hypothesized that in Mesoproterozoic oceans nitrate was limited in offshore environments by low trace metal concentrations and high rates of denitrification in anoxic and episodically euxinic deep water masses, restricting eukaryotes to near-shore environments and limiting their evolutionary innovation. To date this hypothesis has only been tested in the Belt Supergroup (~1.4 Ga), with results that support an onshore-offshore nitrate gradient as a potential control on eukaryote ecology. Here we present bulk nitrogen and organic carbon isotopic data from non-isochronous cross-basinal facies across the Bangemall (~1.5 Ga) and the Roper (~1.4–1.5 Ga) basins to better understand the extent and variability of onshore-offshore nitrogen isotope gradients in the Mesoproterozoic. Both basins show an average ~1–2‰ enrichment in δ¹⁵N_{bulk} from deep to shallow facies, with a maximum range from –1‰ offshore to +7.5‰ onshore. Unlike the Belt basin, the Bangemall and Roper basins show some offshore δ¹⁵N_{bulk} values that are enriched beyond the isotopic range associated with biological N₂ fixation alone. This suggests a mixture of aerobic and anaerobic metabolisms offshore. In shallow waters, where δ¹⁵N_{bulk} enrichment peaks, an aerobic nitrogen cycle was evidently operating. Even though isotopic signatures of aerobic nitrogen cycling are seen in all parts of the Bangemall and Roper basins, our data are consistent with a lateral gradient in nitrate availability within the photic zone, with higher concentrations in near-shore environments than offshore. The variability in δ¹⁵N_{bulk} values in each depositional environment and the consistently low δ¹⁵N_{bulk} values from Mesoproterozoic units compared to the Paleoproterozoic and Neoproterozoic suggest that nitrate concentrations in the global ocean were likely low. This trend is now seen in all three Mesoproterozoic basins so far examined, and contrasts with the Paleoproterozoic and Neoproterozoic where nearly all δ¹⁵N_{bulk} data plot above the N₂ fixation window. Thus, we propose that the Mesoproterozoic ocean was characterized by a nitrate minimum, with the lowest concentrations in offshore environments. This inference is consistent with a Mesoproterozoic O₂ decline following a temporary Paleoproterozoic O₂ peak, and it further supports the idea that nitrate limitation offshore may have contributed to the restriction of photosynthetic eukaryotes to near-shore environments, delaying their rise to ecological dominance until the Neoproterozoic Era.

© 2016 Elsevier Ltd. All rights reserved.

Keywords: Mesoproterozoic; Nitrogen isotopes; Eukaryote evolution; Onshore-offshore gradients

* Corresponding author.

E-mail address: koehlerm@uw.edu (M.C. Koehler).

1. INTRODUCTION

Fixed nitrogen, including nitrate and ammonium, is an essential nutrient for eukaryotes. Its scarcity under certain oceanic redox and chemical conditions may have exerted spatial control on eukaryotic diversity and abundance to such an extent (Anbar and Knoll, 2002) that it repressed the evolutionary radiation of eukaryotic primary producers prior to the Neoproterozoic “second rise of oxygen.” Relevant to this hypothesis, Javaux et al. (2001) found that eukaryotic microfossil diversity and abundance in the Mesoproterozoic Roper basin were greater in marine marginal and inner shelf environments than in outer shelf and basinal settings. Buick and Knoll (1999) found a similar trend in acritarchs and prokaryotic microfossils in the Mesoproterozoic Bangemall basin, noting a decrease in taxonomic diversity and numerical abundance offshore. Contemporaneous with these observed microfossil trends are geochemical data in the form of iron-sulfur systematics, Mo and Cr abundances, and sulfur isotopic ratios that suggest that the Mesoproterozoic ocean was characterized by more widespread anoxia and notably more euxinia than any other time after the Great Oxidation Event (Canfield, 1998; Shen et al., 2003; Arnold et al., 2004; Reinhard et al., 2013; Planavsky et al., 2014; Sperling et al., 2015). In fact, Fe-S systematics and $\delta^{34}\text{S}$ measurements throughout the Roper Group suggest inner and distal shelf depositional environments were likely oxic, while basinal shales record prolonged periods of euxinia (Shen et al., 2003). Trace metal concentrations from the same basinal shales corroborate basinal anoxia with extended periods of euxinia, but overlying surface waters were likely at least transiently oxic (Cox et al., 2016). The “bioinorganic bridge hypothesis” (Anbar and Knoll, 2002) links these micropaleontological and geochemical observations, as follows:

- Biological N_2 fixation and assimilation of nitrate are catalyzed by metalloenzymes that contain siderophile or chalcophile elements in their active sites (Godfrey and Glass, 2011).
- During the Mesoproterozoic Era, when the ocean had relatively widespread euxinia (Canfield, 1998; Reinhard et al., 2013; Sperling et al., 2015), N_2 fixation could have been limited in offshore environments by low trace metal concentrations, in particular Mo, due to their incorporation into precipitating sulfide minerals (Anbar and Knoll, 2002).
- This may have restricted photosynthetic eukaryotes to near-shore environments as suggested by microfossil evidence, prompting ecological subordination to cyanobacteria and, as a result, limiting evolutionary diversification (Anbar and Knoll, 2002).

But does this elegant theoretical scenario stand up to the constraints provided by empirical geochemical data? In an initial study, Stüeken (2013) examined nitrogen isotopic ratios along a cross-basinal transect in the Mesoproterozoic Belt Supergroup, USA, and found that $\delta^{15}\text{N}_{\text{bulk}}$ values changed markedly from $\sim 0\text{‰}$ basinward to $\sim +5\text{‰}$ near-shore. This was interpreted as indicating a gradient from

an anaerobic system dominated by N_2 fixation in the open ocean to aerobic nitrogen cycling involving nitrification coupled to partial denitrification in shallow settings. Although ammonium may have been present in the deeper water column in offshore waters, as in the modern Black Sea (Fuchsman et al., 2008), the availability of fixed nitrogen of any form was probably low in the photic zone away from coastal areas (Stüeken, 2013). This would have been biologically significant, because in the modern ocean cyanobacterial phytoplankton commonly outcompete their eukaryotic counterparts where fixed nitrogen is scarce, because (a) only prokaryotes can fix atmospheric N_2 and (b) organisms with smaller cells have a lower nutrient requirement (Lindell and Post, 1995; Latasa and Bidigare, 1998; Karl et al., 2001; Bouman et al., 2011; Fawcett et al., 2011). Also, in modern oceans, the infiltration of phytoplankton biomass by larger cells occurs when total rates of primary production increase and grazing comes to limit production by smaller cells (Poulin and Franks, 2010); thus, small prokaryotic cells would be expected to dominate in off-shore, nutrient-limited environments.

Stüeken (2013), however, examined only one sedimentary basin, leaving much of the Mesoproterozoic ocean unexplored. Here we report nitrogen abundance and isotopic data from two additional basins of roughly equivalent age, the Bangemall (~ 1.5 Ga) and Roper (~ 1.5 – 1.4 Ga) basins of western and northern Australia, respectively. Although cross-basinal transects are not available, stratigraphic profiles through multiple sedimentary sequences provide samples of deep subtidal, shallow subtidal and peritidal facies, allowing offshore-onshore comparisons of relative nitrogen availability and speciation. Thus, they can indicate whether a nitrate constraint on eukaryotic evolution was just a local phenomenon, or more likely a global feature during the Mesoproterozoic.

1.1. Precambrian nitrogen cycling

Nitrogen cycling has been predominantly controlled by the biosphere since the advent of biological N_2 fixation no later than 3.2 billion years ago (Stüeken et al., 2015a), but it has also been influenced by changes in atmospheric and oceanic redox states. For example, the appearance of free O_2 as early as 2.8 Ga (reviewed by Farquhar et al. (2011)) in microbial mats and marine surface waters (Lalonde and Konhauser 2015; Olson et al., 2013) probably spurred the radiation of nitrifying bacteria (Godfrey and Falkowski, 2009) because locally enhanced crustal weathering (Anbar et al., 2007; Wille et al., 2007; Reinhard et al., 2009; Czaja et al., 2010; Kendall et al., 2010; Stüeken et al., 2012; Gregory et al., 2015; Kurzweil et al., 2015) would have led to a greater influx of trace metals such as Fe, Cu, and Mo. Higher O_2 levels combined with increasing micro-nutrient availability would have facilitated the oxidation of ammonium to nitrite and nitrate (reviewed by Buick, 2007; Godfrey and Glass, 2011). Complementary denitrifying bacteria would have been stimulated by the resulting supply of nitrate (Garvin et al., 2009; Godfrey and Falkowski, 2009). The extent of these coupled oxic-suboxic processes can be inferred from the sedimentary record, because they impart

Table 1

List of nitrogen cycle steps that induce large isotope fractionation effects and their respective fractionation factors. Fractionations are expressed as $\delta^{15}\text{N}_{\text{substrate}} - \delta^{15}\text{N}_{\text{product}}$. References: 1. Zhang et al. (2014); 2. Casciotti (2009); 3. Frey et al. (2014); 4. Brunner et al. (2013); 5. Fulton et al. (2012); 6. Fuchsman and Murray (2008); 7. Altabet and Francois (1994); 8. Kessler et al. (2014); 9. Sigman et al. (2009a).

Nitrogen cycle reaction	Fractionation factor	Ref.	Preservation potential
Nitrogen Fixation ($\text{N}_2 \rightarrow \text{N}_{\text{org}} \rightarrow \text{NH}_4^+$)	Mo-nitrogenase: +2‰ to -1‰ Fe- and V-nitrogenase: +6‰ to +8‰	1	Preserved in sediments from nitrogen-limited ecosystems [5]
Ammonium assimilation ($\text{NH}_4^+ \rightarrow \text{R-NH}_2$)	+14‰ to +27‰	2	Not known to be expressed [cf. 5] (Section 5.2)
Nitrification (ammonium oxidation) ($\text{NH}_4^+ \rightarrow \text{NO}_2^-$)	+14‰ to +38‰	2	Quantitative at chemocline [6]; not preserved
Nitrification (nitrite oxidation) ($\text{NO}_2^- \rightarrow \text{NO}_3^-$)	-12.8‰	2	Quantitative at chemocline [6]; not preserved
Nitrate assimilation ($\text{NO}_3^- \rightarrow \text{R-NH}_2$)	+5‰ to +10‰	2	Usually quantitative in photic zone [7]; not preserved
Denitrification ($\text{NO}_3^- \rightarrow \text{N}_2$)	+10‰ to +30‰	3	Non-quantitative in suboxia [8, 9]; preserved in biomass of NO_3^- assimilators [7]
Annamox ($\text{NO}_2^- + \text{NH}_4^+ \rightarrow \text{N}_2 + 2\text{H}_2\text{O}$)	NO_2^- : +16‰ NH_4^+ : +23‰ to +29‰	4	Probably indistinguishable from denitrification [4]

a distinct kinetic fractionation on the nitrogen isotopes of organic matter compared to those imparted by strictly anaerobic nitrogen cycling (Table 1).

Heavy $\delta^{15}\text{N}^{(a)}$ values, greater than those produced by biological N_2 fixation alone and thus interpreted to represent aerobic nitrogen cycling, are known from the late Archean and early Paleoproterozoic before the Great Oxidation Event (Yamaguchi, 2002; Garvin et al., 2009; Godfrey and Falkowski, 2009; Busigny et al., 2013), and from the later Paleoproterozoic (Kump et al., 2011; Godfrey et al., 2013), *i.e.* during and shortly after the proposed O_2 overshoot at 2.3–2.0 Ga (Bekker et al., 2004; Bekker and Holland, 2012; Planavsky et al., 2012; Hardisty et al., 2014; Scott et al., 2014, Fig. 1). This suggests that surface waters at these times contained enough dissolved oxygen to form significant amounts of nitrate, which was then partially denitrified in the water column and assimilated into biomass. Moreover, isotopic profiles from cross-basinal facies show no trends (Godfrey and Falkowski, 2009; Godfrey et al., 2013), indicating that nitrate was available in the most productive zone of the water column in both on-shore and offshore settings. Similar patterns are also evident across Neoproterozoic basins (Ader et al., 2014).

Nitrogen cycling in the Mesoproterozoic, however, was potentially quite different from any other time in Earth's history. It has been predicted that the expansion of euxinic waters after 1.8 Ga (Canfield, 1998; Arnold et al., 2004) would have led to the scavenging of trace metals such as Mo, Cu, and Fe from seawater into sediments by organic compounds or low-temperature sulfide mineral phases (Saito et al., 2003; Reinhard et al., 2013), restricting their availability for use as metal cofactors in aerobic nitrogen cycle reactions (Anbar and Knoll, 2002; Buick, 2007). For example, Mo concentrations may have been as low as 1–10 nM compared to 105 nM today (Reinhard et al., 2013), which may have limited biological N_2 fixation and

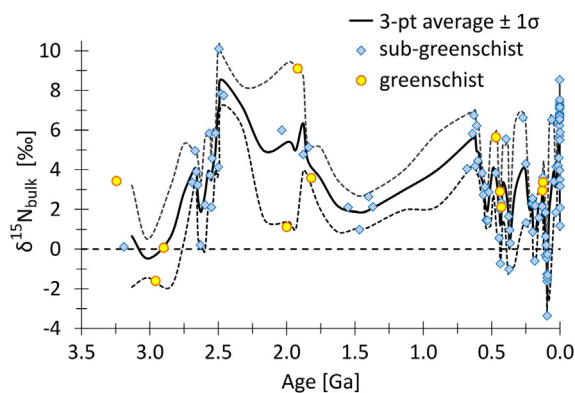


Fig. 1. Average nitrogen isotopic composition of bulk marine sedimentary rocks from offshore environments. Data are compiled from the literature (see Stüeken et al., 2015 for references) and from this study. Each point represents a time-point average, the black solid line marks the running mean over three points. Where no basal gradient is present, all data were used. Samples from hydrothermal cherts and amphibolite facies were excluded.

nitrate assimilation (Zerkle et al., 2006; Glass et al., 2012). This may in turn have delayed the radiation of photosynthetic eukaryotes, which are most productive under a steady supply of nitrate and are incapable of N_2 fixation (Anbar and Knoll, 2002). Nitrate scarcity could have created a positive feedback on trace metal scavenging because it may have spurred microbial sulfate reduction and consequently the expansion of euxinic environments (Boyle et al., 2013). This would have prolonged nitrate limitation until the extent of euxinia contracted (Sperling et al., 2015) possibly through a Neoproterozoic expansion of oxic waters (Canfield and Teske, 1996; Ader et al., 2014; Thomson et al., 2015). For these reasons, much of the Mesoproterozoic ocean may have been unsuitable for eukaryotic life.

Consistent with this idea, the Mesoproterozoic Belt basin displays a distinct onshore-offshore gradient in nitrogen isotopes (Stüeken, 2013). This trend was interpreted to

(a) $\delta^{15}\text{N} = [(^{15}\text{N}/^{14}\text{N})_{\text{sample}} / (^{15}\text{N}/^{14}\text{N})_{\text{standard}} - 1]$, where the standard is atmospheric N_2 .

represent a trend in nitrogen speciation, where nitrate was only available in near-shore environments while an anaerobic nitrogen cycle dominated by N_2 fixation prevailed offshore. A decrease in dissolved oxygen concentration and/or bioessential trace metals in offshore environments probably restricted nitrification to shallow waters (Stüeken, 2013). Any nitrate that was produced offshore was likely consumed rapidly and quantitatively at the chemocline.

2. LOCATION AND GEOLOGICAL SETTING

2.1. Bangemall Supergroup

The Bangemall Supergroup crops out over $\sim 100,000$ km² in northwestern Australia (Fig. 2). Our samples predominantly come from three stratigraphic transects spread over 100 km along the Pingandy Shelf which forms the northern limb of the broad synclinorium in which the Supergroup is now exposed: from west to east Irregully Creek, Wandarray Creek and Fords Creek. These spanned almost the entire ~ 5 km section of the Edmund and Collier Groups, the components of the Supergroup preserved in this region. They largely consist of terrigenous mudrocks and sandstones with subordinate carbonates, cherts and conglomerates. Because of their broad outcrop area and facies relationships, they have been interpreted as entirely (Edmund Group) or dominantly (Collier Group) marine (Martin and Thorne, 2004). Though parts of the Bangemall basin may have been restricted from the open ocean, the Pingandy Shelf, from which the great majority of our samples come, was evidently a long-lived basement high with variable paleo-current patterns (Martin and Thorne, 2004; Martin et al., 2008) suggesting that it was not an isolated and restricted sub-basin. On the Pingandy Shelf, deformation has been modest with only broad open folding during the Mutherbukin Tectonic Event, the Edmundian Orogeny, and the Mulka Tectonic Event (Zi et al., 2015). Several episodes of dolerite sill intrusion occurred during the Mesoproterozoic, causing local contact metamorphism of

siliceous dolomites to talc-tremolite-calcite assemblages in aureoles about 100 m across (Buick et al., 1995). Otherwise metamorphism has been insignificant with kerogen color grading from orange-brown in the east to mid-brown in the west indicating a temperature gradient from 100–125 °C to ~ 150 °C towards the western closure of the synclinorium (Buick and Knoll, 1999).

The Bangemall rocks studied here range in age from between 1680 and 1610 Ma at the base of the stratigraphic section (Zi et al., 2015) to slightly older than 1070 Ma at the top (Martin, 2002; Wingate, 2002; Martin et al., 2008), though most samples come from the >1465 Ma Edmund Group (Wingate, 2002). Their depositional environments ranged from a peritidal carbonate platform in the Irregully Formation at the base through arenaceous siliciclastic shelf sediments containing scattered stromatolitic bioherms in the overlying Gooragoora, Blue Billy, Cheyne Springs, Kiangi Creek and Muntharra Formations, to off-shore delta-front and turbiditic deposits of the Discovery, Devil Creek, and Ullawarra Formations (Martin and Thorne, 2004). The peritidal facies are characterized by silicified dolostones interbedded with green shale and cross-bedded sandstone, forming meter-thick transgressive cycles that pass upward from wavy laminated microbialites with intra-clast breccias and teepee structures through stratiform, pseudocolumnar and muricate (linked conical) stromatolites to large bulbous stromatolites (Buick et al., 1995; Buick and Knoll, 1999). The shallow subtidal facies comprises unsilicified dolostone lenses among coarse-to-fine cross-bedded sandstones, siltstones and grey shales, with conical, domical and columnar stromatolites often on a gigantic scale up to 10 m high and 5 m broad. The deeper subtidal sediments deposited offshore commence with black kerogenous and sulfidic shale and chert but are dominated by siltstone and grey-green shale with minor fine sandstone and nodular to laminated dololite and calcilite, with stromatolite fragments only occurring in breccia lenses.

In terms of geobiological context, $\delta^{13}C_{carb}$ values are remarkably invariant throughout the section, averaging $-0.5\text{‰} \pm 1.3\text{‰}$ (Buick et al., 1995). The only significant deviation from such values occurs in the contact metamorphic aureoles around dolerite sills, where $\delta^{13}C_{carb}$ can go down to -8.4‰ . However, as these rocks are bleached and kerogen-free, they were not analyzed in the current study. As noted above, stromatolites are ubiquitous in the peritidal facies, abundant and gigantic in the shallow subtidal facies but present only as breccia fragments in the deeper offshore facies. Microfossils are often preserved in early diagenetic chert nodules within the peritidal stromatolites, recording benthic mat communities of small filamentous and coccoid prokaryotes (the *Siphonophycus-Sphaerophycus-Eosynechococcus-Myxococcoides-Palaeopleurocapsa* assemblage of Buick and Knoll, 1999). In the shallow subtidal facies, large non-matting filaments and planktonic sphaeromorph acritarchs with thin walls and moderate dimensions are preserved in grey shale (the *Siphonophycus-Leiosphaeridia-Pterospermopsisimorpha-Satka* assemblage of Buick and Knoll, 1999). In offshore kerogenous cherts and shales, only very large chuarid acritarchs with thick multilamellate walls (the *Crassicorium* assemblage)

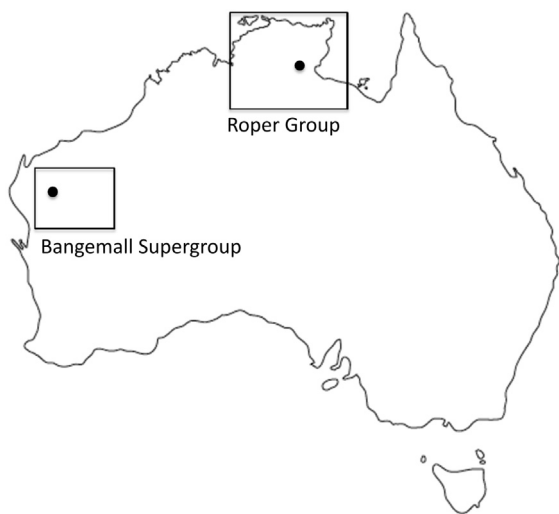


Fig. 2. Locations of the Bangemall Supergroup and Roper Group (boxes) and the approximate locations of sample collection (dots).

are preserved, their complex ultrastructure indicating that they were eukaryotic (Buick and Knoll, 1999). Relevant to nitrogen isotopes, *Palaeopleurocapsa* in the peritidal facies is morphologically similar to an extant genus of N₂-fixing cyanobacteria.

2.2. Roper Group

Samples from the roughly coeval Roper Group from northern Australia were also analyzed in this study. These rocks crop out over 145,000 km² and have a maximum thickness of about 5000 m. Their age ranges from 1492 ± 4 Ma determined by U-Pb in zircon dating for the basal Mainoru Formation (Page et al., 2000) to Re-Os dates of 1361 ± 31 Ma and 1417 ± 29 Ma from the upper Velkerri Formation (Kendall et al., 2009) and a 1429 ± 31 Ma Rb-Sr date from the McMinn Formation at the top of the section (Kralik, 1982). The size of the basin, the abundance of glauconite and sulfide minerals, and sedimentary features indicative of strong tidal influence have been interpreted as indicating open exchange with the global ocean (Jackson and Raiswell, 1991). Sediments are predominantly siliciclastic, ranging from mudrock to sandstone, that were deposited in six progradational cycles (Abbott and Sweet, 2000). High degrees of pyritization, large fractionations in sulfur isotopes and relatively small molybdenum isotope fractionations in black shales indicate that anoxia was pervasive; euxinia was at least transient in deeper parts of the basin and was possibly common along continental margins globally at this time (Jackson and Raiswell, 1991; Shen et al., 2003; Arnold et al., 2004; Johnston et al., 2008; Kendall et al., 2009; Sperling et al., 2015; Cox et al., 2016). In many areas, the rocks are essentially unmetamorphosed, having never been exposed to temperatures above the oil window (Jackson et al., 1988).

The Roper Group is richly fossiliferous (Peat et al., 1978), with microfossil assemblages displaying onshore to offshore trends of decreasing abundance and diminishing diversity (Javaux et al., 2001). There are abundant acritarchs with ultrastructure and ornamentation indicative of eukaryotic affinities (Javaux et al., 2004). In support of this conclusion, kerogen and “live” oil from shales and fluid inclusions yield diverse sterane hydrocarbon biomarkers derived from eukaryotes (Summons et al., 1988; Dutkiewicz et al., 2003, 2004; Volk et al., 2005; Siljeström et al., 2013; but see Flannery and George, 2014 for a contradictory finding), though most biomarkers are of prokaryotic origin. Sulfur isotope studies suggest that some of these prokaryotes metabolized by sulfate reduction (Donnelly and Crick, 1988) and sulfur disproportionation (Johnston et al., 2008).

We obtained samples capturing a range of facies from the tide-dominated inner shelf platform, the storm-dominated outer shelf, and from the deep basin (Abbott and Sweet, 2000). The tide-dominated inner shelf platform comprises sandstones interbedded with mudstones and ooidal ironstones from a *coastal sand platform*; medium-bedded fine to coarse quartz sandstones with trough cross-stratification and ripple marks from a *tide-dominated shoreline*; and medium to thickly bedded sandstones that are massive or have swaley/hummocky

cross-stratification from a *sand-dominated shelf*. The *storm-dominated shelf* consists of thinly interbedded sandstone, mudstone, and siltstone with ripple cross-laminae and small scours, or interlaminated siltstone and mudstone with minor very fine-grained sandstone. *Basinal* samples comprise interbedded mudstones and siltstones. The samples came from four drill cores: Golden Grove 1 (GG1), Broughton 1 (Br1), Urapunga 4 (U4), and Amoco 82/3 (A82/3). Samples from the Mainoru, Crawford, and Hodgson Formations represent one of the six coarsening-upward progradational cycles; samples from the Corcoran and Velkerri Formations are from two separate, overlying cycles (Abbott and Sweet, 2000).

3. ANALYTICAL METHODS

3.1. Sample preparation for bulk rock analyses

Sample preparation followed the methods of Stüeken (2013). Samples were first crushed into centimeter-sized chips using equipment that was thoroughly cleaned with methanol and 18 Ω Milli-Q deionized water. These chips were then sequentially cleaned in an ultrasonic bath with hexane, methanol and deionized water for 10 min each to remove modern organic contaminants. The samples were then dried in a fume hood. Next, the chips were pulverized into a fine powder using an aluminum oxide ceramic puck mill that was cleaned with deionized water, methanol, and pre-combusted silica sand between samples. The powder was treated with 6 M HCl in three iterations (one per day) to dissolve all the carbonate, and then rinsed with deionized water in three more iterations to remove all of the acid. The samples were then left to dry in an oven (60 °C) for two days. The carbonate content was determined gravimetrically as the difference in mass between the untreated and the decarbonated powder aliquot.

3.2. Kerogen extraction for organic nitrogen

During early diagenesis, mineralization can liberate NH₄⁺ from organic compounds, and pore-water NH₄⁺ can then be sorbed by clay minerals through substitution for potassium, due to their similar ionic radii. There is still no consensus on whether bulk analyses (kerogen + silicate-bound nitrogen) or kerogen isolate analyses better record the primary isotopic signals in sedimentary rocks, but due to the low metamorphic grade of these samples (Section 5.1.4), it could be that bulk analyses better reflect primary processes, as kerogen seems to be more susceptible to metasomatic alteration (reviewed in Stüeken et al., 2016). However, we further extracted the kerogen from a subset of samples where enough powder was available to quantify the relative proportions and isotopic compositions of organic-bound and silicate-bound nitrogen. The protocol was adapted from Robl and Davis (1993; see also Stüeken et al., 2015a). Around 5 g of rock powder were weighed into a 250 ml Nalgene bottle and decarbonated with 100 ml of 6 N HCl (reagent grade) at 60 °C in a shaking water bath overnight. Removal of CaCO₃ reduces the formation of insoluble calcium fluorides in subsequent steps. The acid was decanted

after centrifugation (45 min at 4000 rpm) and powders were washed once with DI-H₂O (18 MΩ). Then the silicate matrix was dissolved with a mixture of DI-H₂O (100 ml) and concentrated HF (100 ml, reagent grade) at 60 °C in the shaking water bath overnight. The acid was again decanted after centrifugation. Residual fluoride precipitates were removed by treating the sample with a mixture of H₃BO₃ (62.5 g, reagent grade), DI-H₂O (100 ml) and concentrated HF (100 ml) at room temperature in the shaking water bath overnight. After decanting the acid, the sample was washed three times with 200 ml DI-H₂O, poured into a pre-combusted (500 °C overnight) scintillation vial with 10 ml of DI-H₂O, and placed into a freeze-drier for two days to remove excess water. Nalgene bottles were washed with soap, boiled in bleach for several hours, refluxed with concentrated HCl and methanol overnight, thoroughly rinsed with DI-H₂O, and dried in a clean, closed oven between samples.

3.3. Isotopic analyses

Isotopic compositions ($\delta^{15}\text{N}_{\text{bulk}}$, $\delta^{15}\text{N}_{\text{ker}}$ and $\delta^{13}\text{C}_{\text{org}}$) were determined using a Costech ECS 4010 Elemental Analyzer coupled to a Thermo Finnigan 253 continuous flow isotope-ratio mass spectrometer. $\delta^{13}\text{C}$ values are reported in standard delta notation relative to Vienna PeeDee Belemnite (VPDB). Three in-house standards (two glutamic acids “GA1” and “GA2”, and dried salmon “SA”) calibrated with the international reference materials USGS40 and USGS41 (Qi et al., 2003) were used to calibrate isotope measurements. Another in-house standard from the late Archean Mt. McRae formation (UW McRae) was analyzed in every run as a test for long-term precision (Stüeken et al., 2015a). Analytical blanks resulting from the combustion process were monitored and subtracted for nitrogen isotope measurements; carbon backgrounds were insignificant. The average analytical accuracy of $\delta^{15}\text{N}$ among the individual runs based on the calibrated in-house standard “GA1” was $0.12 \pm 0.09\text{‰}$ (1σ). A similar test for accuracy in $\delta^{13}\text{C}_{\text{org}}$ measurements based on the calibrated in-house standard “SA” was $0.08 \pm 0.10\text{‰}$ (1σ). The average analytical precision of $\delta^{15}\text{N}$ and $\delta^{13}\text{C}_{\text{org}}$ among all runs based on the in-house standard “UW McRae” was 0.15‰ (1σ) and 0.13‰ (1σ) respectively. The average standard deviation between sample replicates was 0.31‰ for $\delta^{15}\text{N}$ and 0.09‰ for $\delta^{13}\text{C}_{\text{org}}$. Replication is the largest source of analytical uncertainty, and so it is used to represent the error of individual sample analyses. Nearly all samples were analyzed at least twice, except in cases where we were sample-limited. Samples where the $\delta^{15}\text{N}$ values varied by more than 0.5‰ or that had a nitrogen sample/blank ratio of less than 5 were replicated further to ensure no analytical biases.

4. RESULTS

4.1. Bangemall basin

Bulk $\delta^{15}\text{N}$ values in the Bangemall basin have a maximum range from -1‰ to $+7.5\text{‰}$ with a modest trend towards lower $\delta^{15}\text{N}_{\text{bulk}}$ values offshore, higher $\delta^{15}\text{N}_{\text{bulk}}$ values near-shore, and variable $\delta^{15}\text{N}_{\text{bulk}}$ values in peritidal envi-

ronments (Table 2). Each of the three stratigraphic sections (Fords Creek, Irregularly Creek, and Wandarray Creek; Fig. 3) shows these characteristics (Table 3). Because the three sections cover equivalent facies, we normalized them with respect to the thickness of the shallow subtidal facies described by Buick et al. (1995) and plotted a composite sequence of $\delta^{15}\text{N}_{\text{bulk}}$ values from deep to peritidal environments shown in Fig. 3. Using all analyses from this composite transect, plus a few additional samples from other localities, the average $\delta^{15}\text{N}_{\text{bulk}}$ value is $+3.3\text{‰} \pm 1.8\text{‰}$ ($n = 18$) for the peritidal facies, $+3.4\text{‰} \pm 1.4\text{‰}$ ($n = 26$) for the shallow subtidal facies, and $+1.8\text{‰} \pm 1.6\text{‰}$ ($n = 28$) in the deep water facies. Both the peritidal and shallow subtidal environments are statistically heavier than the basinal environment ($p_{\text{one-tailed}} = 0.003$ and 0.00008 respectively), though peritidal and shallow subtidal $\delta^{15}\text{N}_{\text{bulk}}$ values are not statistically different from one another ($p_{\text{one-tailed}} = 0.67$). The isotopic composition of kerogen isolates match well with the measured $\delta^{15}\text{N}_{\text{bulk}}$ values (average difference of 0.8‰ among replicated samples) (Table 4), which indicates that the observed gradient is not an artifact of mixing between isotopically distinct nitrogen reservoirs ($\text{N}_{\text{kerogen}}$ and $\text{N}_{\text{silicate}}$). The average total organic carbon [%] and total nitrogen [%] for the Bangemall Group samples are 0.25% , and 0.01% respectively (See Table 2).

The same set of samples has $\delta^{13}\text{C}_{\text{org}}$ values that mostly range from -25‰ to -35‰ . We found a slight basinal gradient of about 3‰ with lighter $\delta^{13}\text{C}_{\text{org}}$ in samples deposited in deeper subtidal environments (Table 5). Samples from each depositional environment come from statistically different $\delta^{13}\text{C}_{\text{org}}$ populations ($p_{\text{anova}} = 0.002$).

4.2. Roper basin

The Roper basin has $\delta^{15}\text{N}_{\text{bulk}}$ values ranging from -1‰ to $+4.9\text{‰}$ with a facies-dependent trend from lighter values in basinal and storm-dominated shelf samples to heavier values in tide-dominated platform samples (average gradient in Tables 3, all data in 6). The mean $\delta^{15}\text{N}_{\text{bulk}}$ value in the tide-dominated platform environment is statistically different from that of the storm-dominated shelf and basinal environments ($p_{\text{one-tailed}} = 0.008$ and 0.0005 respectively). The storm-dominated shelf and basinal $\delta^{15}\text{N}_{\text{bulk}}$ populations are statistically indistinguishable from one another ($p_{\text{one-tailed}} = 0.27$). The average total organic carbon [%] and total nitrogen [%] for the Roper Group samples is 0.34% , and 0.02% respectively (See Table 6).

Unlike the Bangemall Group, the Roper Group shows no sign of a trend in $\delta^{13}\text{C}_{\text{org}}$ across the basin (total average $-31.3\text{‰} \pm 1.55\text{‰}$, $n = 34$, Table 5). Again, kerogen isolates are very similar to bulk samples with an average deviation from the $\delta^{15}\text{N}_{\text{bulk}}$ values of 0.6‰ for replicated samples (Table 4).

5. DISCUSSION

5.1. Diagenesis and metamorphism

5.1.1. Oxidic diagenesis: effects on preserved $\delta^{15}\text{N}_{\text{bulk}}$

Diagenesis under oxidic conditions may increase $\delta^{15}\text{N}_{\text{bulk}}$ by as much as $+4\text{‰}$ (Freudenthal et al., 2001; Lehman

Table 2
New data from the Bangemall Group.

Sample ID	Position [m]	Facies	TN [ppm]	$\delta^{15}\text{N}_{\text{bulk}}$ [‰]	$1\sigma \delta^{15}\text{N}$ [‰]	TOC [ppm]	$\delta^{13}\text{C}_{\text{org}}$ [‰]	$1\sigma \delta^{13}\text{C}$ [‰]	C/N [atomic]	$\delta^{13}\text{C}_{\text{carb}}$ [‰]	Carb [%]
<i>Fords Creek</i>											
89023	73.95	Peritidal	46	4.1	0.30	299	−31.8	0.00	7.6	0.8	72.3
89025	95.7	Peritidal	1719	5.4		4249	−29.6		2.9	0.4	89.1
89028	112.5	Peritidal	50	0.3	0.57	3454	−31.2	0.11	81.0		
89029	122.7	Peritidal	582	3.9		1226	−29.6		2.5	1.2	79.1
89036	160.1	Peritidal	661	3.4		2028	−26.8		3.6	−0.3	89.7
89064	207.63	Shallow	10	2.9	0.15	415	−28.4	0.00	50.9	−0.1	90.9
89071	418.32	Shallow	244	3.7	0.03	7100	−20.8	0.05	34.0	−0.9	86.9
89072	419.34	Shallow	127	3.8	0.22	5005	−26.0	0.17	45.9	−0.5	32.2
89074	431.39	Shallow	64	3.5	0.25	1705	−30.1	0.03	30.9	−1.2	22.8
89075	449.08	Shallow	22	3.5	0.15	291	−27.7	0.13	15.7	−0.6	84.2
89081	511.94	Shallow	217	5.6		7094	−28.5		38.2	−1	95.4
89083	519.53	Shallow	3390	6.7		17847	−28.6		6.1	−0.7	
89086	578.71	Shallow	81	3.3	0.66	850	−28.6	0.13	12.2	0.4	96.7
89090	642.17	Deep	58	2.6	0.53	1705	−30.8	0.05	34.6	0.1	77.6
89091	653.91	Deep	66	4.0	0.81	213	−29.3	0.27	3.8	−0.7	81.5
89093	671.66	Deep	124	2.5		3261	−28.9		30.7	−0.8	97.0
89094	683.4	Deep	94	1.6	0.24	2134	−32.7	0.05	26.5	−1.1	
89095	702.15	Deep	47	5.3	0.26	377	−28.9	0.27	9.3	−1.1	82.3
89097	722.85	Deep	57	3.0	0.11	459	−31.4	0.14	9.4	−1	75.9
89098	733.77	Deep	68	2.8	0.00	447	−30.3	0.11	7.7	−0.8	71.6
89100	753.72	Deep	48	4.9	1.32	701	−29.6	0.15	17.0	−1.2	91.2
89102	764.08	Deep	66	3.1	0.04	414	−30.1	0.08	7.3	−1.3	86.1
89106	873	Deep	64	0.9	0.15	4107	−33.5	0.01	74.6	0.2	57.9
89107	882.4	Deep	21	−0.9	0.93	999	−35.3	0.02	55.1	0.1	63.2
89108	892.79	Deep	90	2.6	0.16	9569	−34.5	0.02	123.6	1.1	46.0
89110	906.7	Deep	19	2.1	0.31	127	−27.8	0.08	7.8	−0.8	
89122	587.2	Shallow	46	1.9	0.32	1963	−30.0	0.04	49.4	−0.6	
89123	538.5	Shallow	35	2.1	0.55	3654	−33.5	0.03	122.7	−1.1	59.5
89125	458.2	Shallow	265	5.5	0.43	456	−27.9	0.65	2.0	0.3	84.6
89127	141.3	Peritidal	86	3.9		2157	−27.9		29.3	0.4	94.4
89130	65.4	Peritidal	78	2.7		1908	−28.5		28.7	0.8	97.5
90049	534.15	Shallow	804	3.7		3639	−32.8		5.3	−0.5	85.5
89028A	112.5	Peritidal	1164	2.8		3058	−28.3		3.1	0.8	
89030D	127.9	Peritidal	52	1.4	0.46	3273	−29.9	0.08	73.9	0.4	92.6
<i>Irregularly</i>											
89165	254.91	Peritidal	430	4.2	0.39	2190	−26.7	0.23	5.9	−0.7	88.1
89166	265.24	Peritidal	88	5.0		2749	−25.1		36.6	−0.2	95.8
89174	308.06	Peritidal	66	−0.2	0.07	1176	−26.0	0.12	20.8	0	96.8
89178	317.94	Peritidal	89	3.4		3905	−26.4		51.0	0.2	96.8
89197	369.81	Peritidal	58	3.8	0.02	2348	−25.9	0.05	47.1	−0.3	90.5
89222	1190.9	Shallow	69	3.8	0.00	1413	−29.0		23.9	−2.1	73.7
89225	1211.94	Shallow	54	3.5	0.01	688	−27.4	0.21	14.8	0.6	56.0
89226	1220.24	Shallow	49	2.7	0.38	664	−30.0	0.05	15.7	0.2	
89231	1243.19	Shallow	905	3.1		953	−31.1		1.2	−0.7	69.8
89232	1252.45	Shallow	72	3.7	0.15	1467	−31.2	0.02	23.9	−0.8	
90010	1914.35	Shallow	374	3.3		23856	−28.3		74.5	−3.9	99.4
90017	1982.17	Deep	104	0.4	0.20	292	−25.2	0.10	3.3	−0.3	46.8
90018	1983.53	Deep	272	1.0	0.15	259	−27.3	0.04	1.1	−1.3	
90019	1993.14	Deep	389	1.0	0.19	2654	−29.8	0.08	8.0	1.6	
90020	2003.25	Deep	244	0.3	0.11	498	−27.1	0.26	2.4	−0.7	52.5
90032	2496.22	Deep	398	2.9	0.44	2008	−32.5	0.18	5.9	−2.8	68.5
<i>Wandarray</i>											
90062	61.64	Peritidal	61	2.6	0.04	1346	−26.8	0.01	25.8	−0.7	94.6
90088	77.72	Peritidal	495	7.5	0.89	2604	−25.0	0.05	6.1	0	77.9
89138	143.9	Peritidal	8	2.3	0.20	507	−22.1	0.65	73.9	0.5	38.5
90070	267.17	Peritidal	5	2.6	0.40	432	−18.7	0.03	105.5	−0.4	13.1
90080	507	Shallow	35	3.6	0.11	423	−28.7	0.01	13.9	−1.1	89.1
90078	519.45	Shallow	33	3.2	0.29	741	−29.8	0.03	26.2	−1.4	89.9
90081	524	Shallow	39	4.0		586	−28.8		17.7	−1.2	94.4

(continued on next page)

Table 2 (continued)

Sample ID	Position [m]	Facies	TN [ppm]	$\delta^{15}\text{N}_{\text{bulk}}$ [‰]	$1\sigma \delta^{15}\text{N}$ [‰]	TOC [ppm]	$\delta^{13}\text{C}_{\text{org}}$ [‰]	$1\sigma \delta^{13}\text{C}$ [‰]	C/N [atomic]	$\delta^{13}\text{C}_{\text{carb}}$ [‰]	Carb [%]
90079	525.25	Shallow	4187	5.4	0.40	9907	−29.6	0.11	2.8	−1.1	93.8
90086	1006.4	Shallow	20	1.2	0.43	304	−28.2	0.21	17.5	0.5	89.9
90087	1018.45	Shallow	671	3.7	0.38	5767	−29.1	0.08	10.0	1.3	92.5
90085	1037.75	Deep	690	0.7	0.30	1015	−31.3	0.10	1.7	1.2	70.3
90084	1038.8	Deep	116	2.1	0.47	537	−32.6	0.06	5.4	−0.6	57.0
90082	1042.75	Deep	94	1.8	0.14	442	−31.9	0.01	5.5	−0.1	46.4
90083	1050	Deep	527	2.9	0.32	648	−31.2	0.05	1.4	−0.7	63.3
<i>Other</i>											
90074		Shallow	41	0.1	0.22	5272	−33.8	0.03	150.4		
89063		Deep	71	0.1		4433	−32.0		72.4		7.1
89066		Deep	52	−1.3		26252	−33.1				6.9
89067		Deep	90	0.0		9119	−31.4		118.8		7.7
90016		Deep	139	1.8	0.04	7342	−30.6	0.05	61.7		
89050		Deep	95	1.7	0.31	306	−23.6	0.07	3.7	−1.8	42.2
89051		Deep	80	1.9	0.27	277	−23.8	0.17	4.0	−2.2	57.3

et al., 2002) due to kinetic fractionation of nitrogen isotopes in favor of ^{14}N during the deamination of organic matter (Macko and Estep, 1984), followed by oxidation and loss of the resulting light inorganic nitrogen (Freudenthal et al., 2001; Robinson et al., 2012). We have no quantitative evidence to completely rule out any effect of oxic diagenesis; however it could not by itself explain the full ranges of $\delta^{15}\text{N}_{\text{bulk}}$ values we observe in the Bangemall (8‰) and Roper (6‰) groups, which are greater than the maximum range known to be caused by aerobic diagenesis. Furthermore, in the absence of bioturbation, middle Proterozoic sediments should have been largely anoxic even under an oxic water column. Hence the effects would likely have been much smaller than in modern sediment profiles (Freudenthal et al., 2001). In thin sections from the Bangemall Group, shallow sediments show no evidence of being more oxidized than deeper equivalents. In particular iron oxides, which have a lower redox potential than nitrate and should thus have formed if pore fluids that were oxidizing enough for nitrification, are absent in both facies. Therefore, a systematic bias of shallow oxic and deep anoxic diagenetic isotope effects is unlikely to be the reason for the basal gradients in $\delta^{15}\text{N}_{\text{bulk}}$.

5.1.2. Anoxic diagenesis: effects on preserved $\delta^{15}\text{N}_{\text{bulk}}$

Anoxic diagenesis can decrease the $\delta^{15}\text{N}_{\text{bulk}}$ of bulk nitrogen in sediments through either the addition of ^{15}N -depleted biomass from in-situ growth of anaerobic bacteria (Lehman et al., 2002), or if organic compounds with relatively higher $\delta^{15}\text{N}$ values such as proteins (Macko et al., 1987) are preferentially degraded, releasing isotopically heavy NH_4^+ into pore waters. However, neither of these mechanisms should have introduced a basal gradient, because as noted above all sediment samples in this study likely underwent anoxic diagenesis regardless of the redox state of the overlying water column. Indeed if anoxic diagenesis caused addition of light N_{org} from bacterial growth, derived from N_2 fixation or the preservation of its isotopic signal (Lehman et al., 2002), then preferential growth of those organisms in deeper environments would only support our interpretation of offshore nitrate depletion

(discussed below). We can further address the latter mechanism, *i.e.* preferential ^{15}N loss from degrading biomass, by comparing bulk $\delta^{15}\text{N}$ values to the $\delta^{15}\text{N}$ values of kerogen isolates. This diagenetic pathway should have led to an isotopic enrichment in silicate minerals that absorbed some of the dissolved heavy NH_4^+ . Hence the $\delta^{15}\text{N}$ of the kerogen isolate from a sample should be systematically lighter than its bulk value, which is not observed. In fact, the Roper and Bangemall kerogen analyses show a very slight average isotopic enrichment of +0.6‰ and +0.8‰, respectively, over the bulk analyses (Table 2). These data may be best explained if NH_4^+ release did not lead to a net isotopic fractionation, perhaps because the effects of kinetic fractionation during deamination (Macko and Estep, 1984) and relative compound instabilities (*cf.* Macko et al., 1987) were roughly balanced. Bulk sediment values are therefore probably close to the original isotopic composition of biomass.

5.1.3. Diagenetic effects on the $\delta^{13}\text{C}$ of organic matter

Both aerobic and anaerobic diagenesis mildly decrease the $\delta^{13}\text{C}$ of organic matter to a maximum of $\sim 1.6\text{‰}$ (Freudenthal et al., 2001; Lehman et al., 2002), probably due to preferential degradation of isotopically heavy organic compounds. Carbohydrates and proteins, which are more susceptible to microbial degradation under both oxic and anoxic conditions, tend to be more enriched in $\delta^{13}\text{C}$ than other more recalcitrant fractions such as lipids (Lehman et al., 2002). Diagenetic effects can be larger (on the order of $\sim 20\text{‰}$ depending on the substrate) if organic degradation is catalyzed by microbes using the Wood-Ljungdahl pathway, which includes methanogens, methanotrophs, and acetogens (Freude and Blaser, 2016). The range of $\delta^{13}\text{C}_{\text{org}}$ in the Bangemall samples is too large ($\sim 10\text{‰}$) to be explained solely by diagenetic effects that do not involve the Wood-Ljungdahl pathway. The slight gradient from lighter values offshore to heavier values near-shore is similar to the environmental trends seen in other studies spanning the Archean and Proterozoic (Eigenbrode and Freeman, 2006; Bekker et al., 2008; Guo et al., 2013), suggesting that it is a primary feature reflecting differential contributions from varying microbial

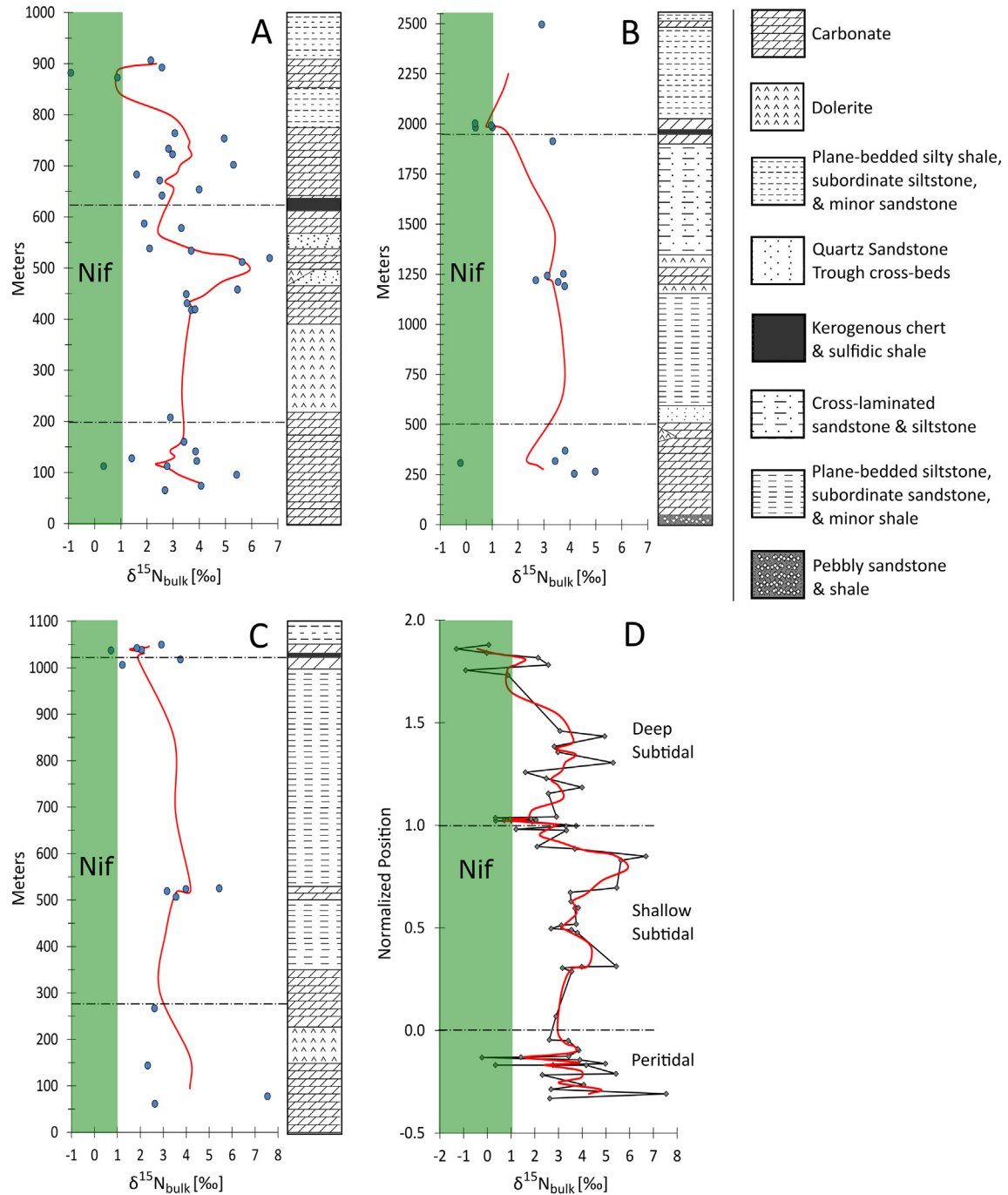


Fig. 3. Stratigraphic $\delta^{15}\text{N}_{\text{bulk}}$ plots of Bangemall transects. (A) Fords Creek, (B) Irregully Creek, (C) Wandarray Creek. Depositional facies in each panel are as in panel (D), with deep subtidal above the top dot-dash line, shallow subtidal in the middle, and peritidal below the bottom dot-dash line. Panel (D) is a normalized compilation of all the Bangemall transects where the positions of each point are relative to the thickness of the shallow subtidal facies. The red line indicates the running mean over three points.

metabolisms in response to local redox conditions (Section 5.2).

5.1.4. Metamorphism

Four lines of evidence indicate that the effects of metamorphism on primary nitrogen isotope signals were probably insignificant. First, as stated previously, both the

Bangemall and Roper rocks were not exposed to temperatures much above the oil window (Jackson et al., 1988; Buick and Knoll, 1999), whereas there seems to be no metamorphic effects on nitrogen isotopes (*i.e.* preferential loss of ^{14}N) in other rocks up through the gas window (Rivera et al., 2015); these may only become important ($>1\%$) at greenschist facies and above (reviewed by Thomazo and

Table 3

$\delta^{15}\text{N}_{\text{bulk}}$ values for the Bangemall basin transects and whole basin, the Roper basin, and the Belt basin. Belt data are from Stüeken (2013). Parenthetical facies labels are specific to the Roper basin. Uncertainties are expressed as $\pm 1\sigma$. n = number of samples.

	Peritidal (tide-dominated platform) $\delta^{15}\text{N}_{\text{bulk}}$	Shallow subtidal (storm-dominated shelf) $\delta^{15}\text{N}_{\text{bulk}}$	Deep subtidal (basinal) $\delta^{15}\text{N}_{\text{bulk}}$
Bangemall basin			
Fords Creek	$3.1\text{‰} \pm 1.5\text{‰}$ ($n = 10$)	$3.9\text{‰} \pm 1.4\text{‰}$ ($n = 12$)	$2.7\text{‰} \pm 1.6\text{‰}$ ($n = 13$)
Irregully Creek	$3.2\text{‰} \pm 2.0\text{‰}$ ($n = 5$)	$3.4\text{‰} \pm 0.4\text{‰}$ ($n = 6$)	$1.1\text{‰} \pm 1.1\text{‰}$ ($n = 5$)
Wandarray Creek	$3.8\text{‰} \pm 2.5\text{‰}$ ($n = 4$)	$3.5\text{‰} \pm 1.4\text{‰}$ ($n = 6$)	$1.9\text{‰} \pm 0.9\text{‰}$ ($n = 4$)
All	$3.3\text{‰} \pm 1.8\text{‰}$ ($n = 18$)	$3.4\text{‰} \pm 1.4\text{‰}$ ($n = 26$)	$1.8\text{‰} \pm 1.6\text{‰}$ ($n = 28$)
Roper basin	$3.7\text{‰} \pm 0.8\text{‰}$ ($n = 6$)	$2.3\text{‰} \pm 1.3\text{‰}$ ($n = 20$)	$2.0\text{‰} \pm 0.8\text{‰}$ ($n = 8$)
Belt basin	$3.7\text{‰} \pm 1.4\text{‰}$ ($n = 13$)	$1.5\text{‰} \pm 1.2\text{‰}$ ($n = 35$)	$0.1\text{‰} \pm 0.9\text{‰}$ ($n = 21$)

Table 4

Kerogen data. Included are data from both the Roper and the Bangemall groups.

Sample ID	$\delta^{15}\text{N}_{\text{kerogen}}$ [‰]	1σ [‰]	C/N _{ker} [atomic]	F (N _{ker}) [%]	F (N _{sil}) [%]*
<i>Bangemall</i>					
90050	2.73		126		
90079	5.87	0.30	39.1	71	29
89138	4.38	0.06	103.2		
89094	2.16	0.20	70.2	40	60
89036	3.22		81.1	44	56
89028	1.27	0.30	97.4	86	14
<i>Roper</i>					
A391.0	4.57	0.55	80.1	24	76
BR1 23.4	2.55		89.8	2	98
BR1 244.7	2.63		110.1	4	96
GG1 53.2	2.86		46.9	18	82
U4 33.2	5.34	0.12	61.0	66	34
U4 82.25	3.55	0.42	68.5	23	77

*To calculate the fraction (F) of silicate and kerogen bound nitrogen:

$$F_{\text{kerogen}} = 1 - F_{\text{Silicate}} = \frac{N[\%]_{\text{kerogen}}}{C[\%]_{\text{kerogen}}} \times \frac{TOC[\%]_{\text{bulk}}}{TN[\%]_{\text{bulk}}}$$

Table 5

$\delta^{13}\text{C}_{\text{org}}$ in the Bangemall, Roper, and Belt basins. Parenthetical facies labels are specific to the Roper basin. Data from the Jixian basin are taken from Guo et al. (2013), and data from the Belt basin are from Stüeken (2013). Uncertainties are expressed as $\pm 1\sigma$. n = number of samples.

	Peritidal (tide-dominated platform) $\delta^{13}\text{C}_{\text{org}}$	Shallow subtidal (storm-dominated shelf) $\delta^{13}\text{C}_{\text{org}}$	Deep subtidal (basinal) $\delta^{13}\text{C}_{\text{org}}$
Bangemall basin	$-27.0\text{‰} \pm 3.2\text{‰}$ ($n = 18$)	$-29.2\text{‰} \pm 2.6\text{‰}$ ($n = 26$)	$-30.2\text{‰} \pm 2.9\text{‰}$ ($n = 28$)
Roper basin	$-31.5\text{‰} \pm 0.9\text{‰}$ ($n = 6$)	$-30.6\text{‰} \pm 1.2\text{‰}$ ($n = 20$)	$-32.9\text{‰} \pm 1.6\text{‰}$ ($n = 8$)
Belt basin	$-32.2\text{‰} \pm 1.2\text{‰}$ ($n = 13$)	$-30.1\text{‰} \pm 1.9\text{‰}$ ($n = 35$)	$-22.9\text{‰} \pm 2.9\text{‰}$ ($n = 21$)
Jixian basin	$-28.2\text{‰} \pm 1.6\text{‰}$ ($n = 191$)	$-30.8\text{‰} \pm 2.0\text{‰}$ ($n = 61$)	n/a

Papineau, 2013). Second, the slight metamorphic gradient from east to west in the Bangemall basin does not parallel, but is nearly perpendicular to, the three transects, but no significant differences are evident between them. Third, if metamorphism did have an effect on the nitrogen isotope ratios of the samples, then increasing $\delta^{15}\text{N}_{\text{kerogen}}$ should correlate with increasing (C/N)_{kerogen} ratios, as nitrogen is more mobile than carbon and ^{14}N is more mobile than ^{15}N under such conditions (Haendel et al., 1986; Bebout and Fogel, 1992; Jia, 2006). However, such correlations are not seen in either sample set (Fig. 4, $R^2 = 0.28$ for Bangemall, and $R^2 = 0.14$ for Roper). Lastly, offsets between $\delta^{15}\text{N}_{\text{silicate}}$ and $\delta^{15}\text{N}_{\text{kerogen}}$ of up to $\sim 12\text{‰}$ have

been observed in rocks within hornfels aureoles (Godfrey and Falkowski, 2009), suggesting there may be a relationship between increasing metamorphic grade and increasingly divergent $\delta^{15}\text{N}_{\text{bulk}}$ and $\delta^{15}\text{N}_{\text{kerogen}}$ values. There is little consensus on whether kerogen or bulk nitrogen better preserves primary biological signals (see Stüeken et al., 2016); however, on average, the kerogen nitrogen isotope values in the Bangemall and Roper Groups fall within 0.7‰ of bulk values, inconsistent with significant metamorphic alteration.

In the case of carbon isotopes, metamorphism also can spur exchange between the carbon in organic matter and the carbon in carbonates, causing $\delta^{13}\text{C}_{\text{carb}}$ to become

Table 6

New data from the Roper Group. Facies abbreviations: t.d shoreline = tide-dominated shoreline; sand.d shelf = sand-dominated shelf; s.d shelf = storm-dominated shelf; c.s platform = coastal sand platform. coastal sand platform, tide-dominated shoreline, and sand-dominated shelf all fall within the broader category of “tide-dominated shelf” as described in Section 2.2 of the main text.

Sample ID	Position [m]	Facies	TN [ppm]	$\delta^{15}\text{N}_{\text{bulk}} [‰]$	$1\sigma \delta^{15}\text{N} [‰]$	TOC [ppm]	$\delta^{13}\text{C}_{\text{org}} [‰]$	$1\sigma \delta^{13}\text{C} [‰]$	C/N [atomic]	Carb (%)	Formation
<i>Amoco 82/3</i>											
A101.5	101.5	t.d shoreline	173	2.7	0.48	5002	-31.9	0.05	33.7	8.5	Bessie Creek
A178.0	178	sand.d shelf	36	4.9	0.61	768	-30.8	0.14	25.0	37.1	Jalboi
A311.3	311.3	s.d shelf	47	-1.0	0.11	978	-30.6	0.01	24.2	20.8	Crawford
A331.8	331.8	s.d shelf	165	2.6	0.39	1434	-29.7	0.05	10.1	21.5	Crawford
A375.1	375.1	s.d shelf	199	2.8	0.36	2369	-30.9	0.03	13.9	28.2	Crawford
A391.0	391	s.d shelf	225	3.8	0.41	3992	-30.8	0.01	20.7	15.1	Crawford
A407.65	407.65	s.d shelf	24	-0.9	1.95	336	-28.4	0.23	16.2	18.1	Crawford
A544.1	544.1	s.d shelf	315	2.7	0.31	2593	-30.2	0.07	9.6	27.7	Maironu
A549.25	549.25	s.d shelf	250	3.6	0.43	1191	-29.8	0.17	5.6	27.1	Maironu
A561.05	561.05	s.d shelf	214	2.7	0.46	596	-28.7	0.03	3.2	29.2	Maironu
<i>Broughton 1</i>											
BR1 23.4	23.4	s.d shelf	429	2.1	0.30	794	-30.3	0.10	2.2	21.0	Corcoran
BR1 34.5	34.5	s.d shelf	222	2.3	0.24	686	-30.4	0.03	3.6	12.6	Corcoran
BR1 42.3	42.3	s.d shelf	253	2.3	0.45	1006	-30.9	0.11	4.6	15.9	Corcoran
BR1 52.35	52.35	s.d shelf	179	1.6	0.27	1023	-30.8	0.08	6.7	30.4	Corcoran
BR1 69.0	69	s.d shelf	289	2.7	0.22	774	-29.8	0.13	3.1	21.4	Corcoran
BR1 122.4	122.4	c.s platform	518	3.3	0.27	1041	-30.0	0.09	2.3	33.5	Hodgsen ss
BR1 136.8	136.8	c.s platform	99	4.0	0.42	2122	-31.7	0.07	24.9	14.4	Hodgsen ss
BR1 150.45	150.45	s.d shelf	217	1.8	0.50	1328	-30.7	0.05	7.1	18.9	Crawford
BR1 244.7	244.7	s.d shelf	227	3.7	0.10	914	-29.5	0.02	4.7	18.7	Maironu
<i>Golden Grove 1</i>											
GG1 48.75	48.75	basinal	160	0.5	0.66	3300	-32.0	0.04	24.1	25.9	Velkerri
GG1 53.2	53.2	basinal	326	1.4	0.10	2373	-31.7	0.07	8.5	19.9	Velkerri
GG1 229.50	229.5	s.d shelf	435	2.9	0.08	1620	-32.3	0.01	4.3	16.1	Corcoran
GG1 370.70	370.7	s.d shelf	346	3.4	0.25	978	-30.5	0.02	3.3	8.9	Corcoran
<i>Urapunga 4</i>											
U4 26.4	26.4	c.s platform	544	3.6	0.42	13617	-32.5	0.07	29.2	31.2	McMinn
U4 33.2	33.2	c.s platform	79	3.9	0.43	3779	-32.1	0.00	56.0	44.2	McMinn
U4 82.25	82.25	basinal	375	2.9	0.32	5092	-32.0	0.10	15.9	19.8	Velkerri
U4 124.0	124	basinal	475	2.6	0.14	23859	-33.8	0.21	58.6	22.2	Velkerri
U4 421.5	421.5	s.d shelf	266	1.7	0.46	1908	-32.4	0.05	8.4	25.5	Corcoran
U4 431.0	431	s.d shelf	432	2.5	0.15	3450	-32.5	0.06	9.3	14.5	Corcoran
U4 440.95	440.95	s.d shelf	285	2.8	0.26	1768	-32.6	0.04	7.2	16.9	Corcoran
U4 485.1	485.1	basinal	227	1.9	0.30	1418	-31.2	0.01	7.3	36.8	Corcoran
<i>Other</i>											
Velkerri_CS11		basinal	1409	2.2	0.13	52629	-34.3	0.01	43.6		Velkerri
Velkerri_CS17		basinal	1287	2.3	0.03	62685	-35.8	0.01	56.8		Velkerri
Velkerri_CS9		basinal	1531	2.2	0.23	42574	-32.7	0.03	32.4		Velkerri

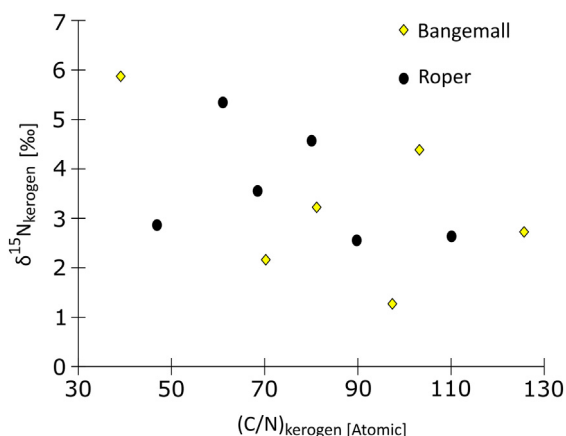


Fig. 4. $\delta^{15}\text{N}_{\text{kerogen}}$ vs. $\text{TOC}/\text{N}_{\text{kerogen}}$ (total organic carbon/kerogen-bound nitrogen) for Bangemall (yellow diamonds) and Roper (black circle) samples. (For interpretation of the references to colour in this figure legend, the reader is referred to the web version of this article.)

depleted by up to 5‰ and $\delta^{13}\text{C}_{\text{org}}$ to become enriched by as much as 15‰ (reviewed by [Schidlowski, 1987](#)). This effect is sensitive to the relative percentages of carbonate to organic carbon. Hence in carbonate-rich sediments such as the Bangemall samples, depletion of the carbonate may not be noticeable but enrichment of organic matter might be prominent. However, fractionations caused by carbon equilibration between organics and carbonates are generally insignificant below greenschist facies ([McKirdy and Powell, 1974](#); [Hoefs and Frey, 1976](#); [Hayes et al., 1983](#)). There is no inverse correlation between the $\delta^{13}\text{C}_{\text{org}}$ and $\delta^{13}\text{C}_{\text{carb}}$ values of the same Bangemall samples ($r^2 = 0.003$), and the total fractionation $\Delta^{13}\text{C}$ ($=\delta^{13}\text{C}_{\text{carb}} - \delta^{13}\text{C}_{\text{org}}$) is not inversely correlated with carbonate content ($r^2 = 0.008$), even in the largest negative excursions of $\delta^{13}\text{C}_{\text{carb}}$. These lines of evidence all suggest the carbon isotopic composition of the samples measured in this study are unaltered by metamorphism.

5.2. Carbon cycling in the Bangemall and Roper basins

The Bangemall basin shows a slight spatial trend in $\delta^{13}\text{C}_{\text{org}}$ values, with relatively lighter values offshore and heavier values near-shore ([Table 5](#)). The $\delta^{13}\text{C}_{\text{org}}$ gradient in the Bangemall basin is thus the opposite to that of the Belt basin ([Stüeken, 2013](#)), where onshore sediments are markedly depleted in $\delta^{13}\text{C}$ compared to offshore sediments ([Table 5](#), $p_{\text{anova}} = 0.0009$). However, a similarly oriented gradient to this study was recently reported from the roughly contemporaneous Jixian Group (1.5 Ga) with values around -28.2‰ onshore and -30.8‰ offshore with $p_{\text{anova}} < 0.0001$ ([Table 5](#), [Guo et al., 2013](#)). Given that $\delta^{13}\text{C}_{\text{carb}}$ is nearly invariable in this and earlier Mesoproterozoic basins ([Buick et al., 1995](#)), this gradient is probably not caused by changes in the isotopic composition of dissolved inorganic carbon, as seen from the later Mesoproterozoic onwards ([Bartley and Kah, 2004](#); [Gilleaudeau and Kah, 2013](#)), but may instead reflect spatial variability in biological fractionation effects. A similar trend was also

observed in the Pretoria and Fortescue Groups, which along with the Jixian Group and Bangemall Group represent the Mesoproterozoic, Paleoproterozoic, and Neoproterozoic. ([Eigenbrode and Freeman, 2006](#); [Bekker et al., 2008](#); [Guo et al., 2013](#)). All $\delta^{13}\text{C}_{\text{org}}$ values in the Bangemall and Roper basins are consistent with autotrophic fixation of CO_2 by the Calvin cycle that is used by a wide range of organisms including cyanobacteria and eukaryotic algae ([Hayes, 2001](#)). However, the fact that multiple basins through time show a similar trend suggests there may be (i) autotrophic carbon fixation under a gradient of nutrient availability, or (ii) photoautotrophic biomass mixed with varying proportions of secondary chemoautotrophic and/or heterotrophic biomass, as proposed for the contemporaneous Belt and Jixian basins ([Guo et al., 2013](#); [Stüeken, 2013](#)). Such secondary metabolisms could include methanogenesis, acetogenesis, and methanotrophy that use the Wood-Ljungdahl pathway and are known to cause large fractionations in carbon isotopes ([Freude and Blaser, 2016](#)). We cannot rule out either possibility, and it is also not clear why the reverse gradient is seen in the Mesoproterozoic Belt basin ([Stüeken, 2013](#)). The samples from the Roper Group do not show a gradient in $\delta^{13}\text{C}_{\text{org}}$ values.

5.3. Nitrogen cycling in the Bangemall and Roper basins

The Bangemall transects and the Roper Group samples all show a $\sim 1.0\text{‰}$ to $\sim 2.0\text{‰}$ gradient in nitrogen isotopes, with lighter values recorded in offshore facies and heavier values in near-shore facies. We note that our results for the deep subtidal/basinal facies of the Bangemall and Roper groups ($+1.8\text{‰} \pm 1.6\text{‰}$, $n = 28$; $+2.0\text{‰} \pm 0.8\text{‰}$, $n = 8$ respectively) are in good agreement with basinal mudstones from the roughly contemporaneous Xiamaling Formation ($\delta^{15}\text{N}_{\text{bulk}} = +2.1 \pm 0.2\text{‰}$, $n = 4$, age 1.37 Ga) ([Luo et al., 2015](#)). The facies-dependent trend in the Bangemall and Roper basins likely reflects primary nitrogen cycling rather than post-depositional alteration (see above), and so is interpreted as being consistent with cross-basin differences in nitrogen speciation, comparable to the Belt basin ([Table 3](#); [Stüeken, 2013](#)). As noted in Section 1, Fe-S systematics, $\delta^{34}\text{S}$, and trace metal data also have facies-dependent trends in the Roper Group, providing evidence for an oxic near-shore water column, and anoxic/euxinic basinal deep waters overlain by at least transiently oxic surface waters ([Shen et al., 2003](#); [Cox et al., 2016](#)). There are no equivalent data for the Bangemall Group, but a similar range of conditions appears to have been widespread in the Mesoproterozoic ocean ([Sperling et al., 2015](#)). These data are consistent with, and indeed support, our interpretation of the nitrogen isotope data which follows.

The lightest $\delta^{15}\text{N}_{\text{bulk}}$ values are most plausibly explained by an ecosystem dominated by N_2 fixation using the molybdenum-bearing nitrogenase Nif ([Zerkle et al., 2008](#); [Nishizawa et al., 2014](#); [Zhang et al., 2014](#)). If the ocean had been fully oxygenated at that time, more so than today, then values around 0‰ could in theory also have been produced by quantitative nitrification of biomass followed by quantitative re-assimilation of nitrate without any denitrifi-

cation and consequent isotopic fractionation in oxygen-minimum zones (Quan and Falkowski, 2009). However, this scenario is unlikely in the mid-Proterozoic, where widespread anoxia has been well documented (Arnold et al., 2004; Planavsky et al., 2011; Poulton and Canfield, 2011; Reinhard et al., 2013; Sperling et al., 2015). An N_2 -fixation dominated regime is thus the most parsimonious explanation for light $\delta^{15}N_{\text{bulk}}$ values in our samples.

Three alternative mechanisms can be considered to explain the isotopically heavy $\delta^{15}N$ values ($>2\text{‰}$) (see Stüeken, 2013; Ader et al., 2016, and Stüeken et al., 2016 for detailed discussion).

- (i) It has been hypothesized that in an anaerobic nitrogen cycle, partial assimilation of an NH_4^+ pool by organisms can leave the residual NH_4^+ pool enriched in ^{15}N , as life preferentially assimilates ^{14}N into biomass (Papineau et al., 2009). If this enriched pool of NH_4^+ is subsequently transported to a different location and assimilated by organisms, two isotopic facies result: the first location preserves light $\delta^{15}N_{\text{bulk}}$ and the second preserves heavy $\delta^{15}N_{\text{bulk}}$.
- (ii) Partial nitrification of NH_4^+ can create a nitrate pool that is depleted in ^{15}N and a residual NH_4^+ pool that is enriched in ^{15}N because nitrification preferentially selects for the lighter isotope. Assimilation of the NH_4^+ pool will result in heavy $\delta^{15}N_{\text{bulk}}$ so long as the light nitrate is removed from the system, either through subsequent complete denitrification or relocation. Partial nitrification is rare in modern water columns, occurring where seasonally fluctuating oxygen concentrations occur in transiently stratified waters (Granger et al., 2011; Morales et al., 2014). However, it is possible that low oxygen concentrations in the Mesoproterozoic enabled more widespread partial nitrification coupled with the removal of the light nitrate pool by complete denitrification. Subsequent uptake of the leftover heavy NH_4^+ and further remineralization of organic matter to NH_4^+ could result in a range of positive $\delta^{15}N_{\text{bulk}}$ values (Stüeken, 2013; Morales et al., 2014).
- (iii) Partial denitrification of a nitrate pool in the water column will leave the residual nitrate enriched in ^{15}N , as the biologically governed steps of denitrification, like nitrification, preferentially use ^{14}N over ^{15}N . So N_2 , the most common end-product of denitrification, would be isotopically depleted in ^{15}N and organisms could assimilate the remaining heavy nitrate pool. This is the mechanism producing heavy $\delta^{15}N_{\text{bulk}}$ in the modern ocean (e.g. Sigman et al., 2009b; Tesdal et al., 2013).

Mechanisms (i) and (ii) should result in two distinct isotopic reservoirs, one that is relatively depleted below -2‰ , and one that is relatively enriched above $+1\text{‰}$. There are no samples or sample sets from this study that are lighter than the $\delta^{15}N_{\text{bulk}}$ values that would result from N_2 fixation by Mo-nitrogenase (-2‰ to $+1\text{‰}$, Zhang et al., 2014). We cannot rule out that a much lighter facies exists somewhere within or adjacent to the Bangemall and Roper basins, but

was not sampled. Nevertheless, explanations (i) and (ii) are unlikely for several reasons. First, the Black Sea, our best modern analog for the Mesoproterozoic ocean, has a large NH_4^+ reservoir in the anoxic bottom water, but underlying sediments do not record evidence of partial NH_4^+ assimilation; values are close to 0‰ , reflecting nitrogen limitation and N_2 fixation in the photic zone (Fulton et al., 2012). The same is true for the modern anoxic Cariaco basin (Haug et al., 1998). This argues against an isotopically light nitrogen reservoir resulting from partial NH_4^+ assimilation in the similarly chemically stratified Mesoproterozoic ocean (option i). Hydrodynamically, the Black Sea and Cariaco basin are probably more stagnant than open marine settings like the Roper and Bangemall basins, and so it is conceivable that these Mesoproterozoic settings experienced a relatively higher upwelling flux of NH_4^+ from deeper waters into the photic zone. In theory, this scenario could favor non-quantitative NH_4^+ assimilation. However, in the modern ocean, NO_3^- assimilation usually goes to completion with minimal net isotopic fractionations because nitrogen is the proximally limiting nutrient (e.g. Tyrrell, 1999; Thunell et al., 2004; Tesdal et al., 2013). There is no *a priori* reason to expect that this would have been different if the nitrogenous compound was NH_4^+ instead of NO_3^- . This is especially true if low Mo levels reduced N_2 fixation rates in the Mesoproterozoic ocean and exacerbated nitrogen limitation (Reinhard et al., 2013). Furthermore, upwelling would have been most pronounced along the continental margin rather than far offshore, and so the hypothetical isotopically light reservoir should be preserved in our sample set, which is not the case. Regarding option (ii), in the Black Sea nitrification quickly goes to completion under suboxic conditions at the chemocline (Fuchsman et al., 2008). The same is true in bacterial cultures and oxygen minimum zones along open marine margins (Füssel et al., 2012; Martens-Habbena et al., 2009; Thamdrup et al., 2012), suggesting that partial nitrification may also have been rare in the past as long as surface waters were at least mildly oxidizing. Indeed, in modern environments partial nitrification requires transient seasonal changes in the environment such as fluctuating sea ice cover and is not known to operate over long geologic timescales. This leaves option (iii), partial denitrification at the chemocline (*cf.* Sigman et al., 2009b) or in sediment pore waters (Kessler et al., 2014) as the most plausible mechanism responsible for heavier $\delta^{15}N_{\text{bulk}}$ values in the shallower facies of the Bangemall and Roper basins. We thus interpret the large variations of $\delta^{15}N_{\text{bulk}}$ in the Bangemall and Roper basins as reflecting differential mixing between components derived from N_2 fixation (alone responsible for the most depleted values between -2‰ and $+1\text{‰}$) and from an aerobic nitrogen cycle coupled with varying degrees of partial denitrification of a nitrate pool followed by nitrate assimilation yielding $\delta^{15}N_{\text{bulk}}$ values above $+1\text{‰}$.

As some peritidal samples have anomalously light $\delta^{15}N_{\text{bulk}}$ values, it may be that N_2 fixation temporarily dominated in microbial mats that were transiently cut off from the marine nitrate pool at low tide, which would be consistent with microfossil evidence from the Bangemall basin peritidal facies, where *Palaeopleurocapsa* (morphologically

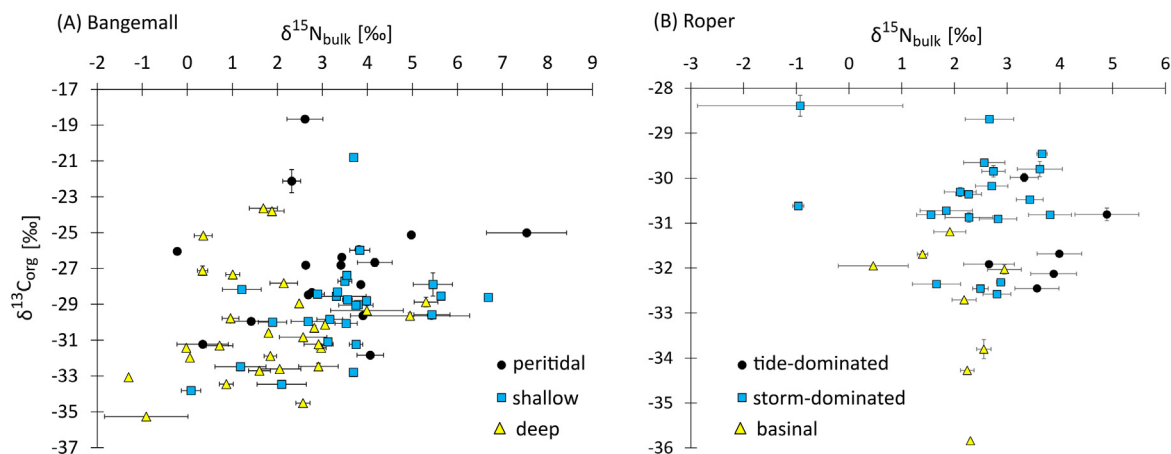


Fig. 5. $\delta^{15}\text{N}_{\text{bulk}}$ plotted against $\delta^{13}\text{C}_{\text{org}}$ for the Bangemall (A) and Roper (B) basins. The plot also includes those samples from the Bangemall basin that do not belong to one of the three main transects shown in Fig. 3A–C. Error bars are $\pm 1\sigma$.

similar to a modern genus of nitrogen-fixing cyanobacteria; Section 2.1) is found (Buick and Knoll, 1999). All shallow subtidal samples have $\delta^{15}\text{N}_{\text{bulk}}$ values above $+1\text{‰}$ (barring one outlier), suggesting that some nitrate was always available in the water column and that there was a permanent chemocline where partial denitrification was occurring. Deep subtidal samples have lower $\delta^{15}\text{N}_{\text{bulk}}$ values than shallow (Table 3) and contain samples within the -2‰ to $+1\text{‰}$ range (Figs. 5 and 6). Almost all deep-water values for both basins are lighter than $+3\text{‰}$, *i.e.* lighter than most modern and recent marine sediments ($>+4\text{‰}$, *e.g.* Sigman et al., 2000; Galbraith et al., 2013; Algeo et al., 2014). This suggests that offshore sites had less nitrate available compared to shallower facies and the modern deep ocean. Thus our data are consistent with at least some nitrate in all depositional environments in both the Bangemall and Roper basins, but relatively more in near-shore facies than offshore. When we discuss nitrate availability, we refer to availability in the zones of highest biological production, as this zone will generate the dominating isotopic signal preserved in sediments. This is probably the photic zone, and it is unlikely that nitrate could have existed much deeper in the water column if bottom waters during the Mesoproterozoic were predominantly anoxic.

5.4. $\delta^{15}\text{N}_{\text{bulk}}$ variability in the Bangemall and Roper basins

The variability of $\delta^{15}\text{N}_{\text{bulk}}$ values in the Bangemall and Roper shallow water facies can be better understood by drawing an analogy to the variability of $\delta^{34}\text{S}$ values proposed for the Proterozoic (Kah et al., 2004). In this conceptual model, the rate of change in the nitrate isotopic composition of shallow water environments is controlled by the size of the nitrate reservoir, and the size and isotopic composition of fluxes that both add and remove isotopically distinct nitrogen. The relationship is as follows, with fluxes labeled in Fig. 7:

$$\begin{aligned} d(\delta_{\text{NO}_3^-})/dt = & (F_{\text{upwell}} \Delta_{\text{upwell}} + F_{\text{nitri.}} \Delta_{\text{nitri.}} + F_{\text{fixation}} \Delta_{\text{fixation}} \\ & - F_{\text{assim}} \Delta_{\text{assim}} - F_{\text{den.sed.}} \Delta_{\text{den.sed.}} \\ & - F_{\text{den.wc.}} \Delta_{\text{den.wc.}}) / M_{\text{NO}_3^-} \end{aligned}$$

$d(\delta_{\text{NO}_3^-})/dt$ is the isotopic rate of change of the shallow water nitrate reservoir. F_{upwell} is the flux of nitrogen being upwelled from deep water environments. Δ_{upwell} is equivalent to $\delta^{15}\text{N}_{\text{NH}_4^+} - \delta^{15}\text{N}_{\text{NO}_3^-}$, which is the isotopic difference of the ammonium being upwelled and the existing shallow water nitrate reservoir. $F_{\text{nitri.}} \Delta_{\text{nitri.}}$ is the isotopic flux term of organic nitrogen that is nitrified within the shallow water environment. $\Delta_{\text{nitri.}}$ is 0 because nitrification likely goes to completion, and will preserve the isotopic composition of shallow water nitrate, from which the organic matter was likely derived. $F_{\text{fixation}} \Delta_{\text{fixation}}$ is the isotopic flux contributed by N_2 fixation in shallow water environments. This flux could contribute to changes in the isotopic composition of shallow water nitrate as Δ_{fixation} equals $\delta^{15}\text{N}_{\text{fixation}} - \delta^{15}\text{N}_{\text{NO}_3^-}$. It may be the case, however, that F_{fixation} is 0 because N_2 fixation was probably negligible onshore where nitrogen was more available. $F_{\text{assim}} \Delta_{\text{assim}}$ is the isotopic flux of nitrogen being assimilated by shallow water organisms. This is likely also 0, as there is no evidence for non-quantitative assimilation (negative $\delta^{15}\text{N}_{\text{bulk}}$ values). $F_{\text{den.sed.}} \Delta_{\text{den.sed.}}$ is the isotopic flux associated with sedimentary denitrification. $\Delta_{\text{den.sed.}}$ is also close to 0, as sedimentary denitrification does not impart large isotopic fractionations on the nitrate in the overlying water column (Kessler et al., 2014; Rooze and Meilie, 2016). $F_{\text{den.wc.}} \Delta_{\text{den.wc.}}$ is the isotopic flux from canonical water column denitrification. $\Delta_{\text{den.wc.}}$ is around 20‰ . $M_{\text{NO}_3^-}$ is the total onshore nitrate reservoir in grams or moles. Removing the 0 terms, we are left with:

$$d(\delta_{\text{NO}_3^-})/dt = (F_{\text{upwell}} \Delta_{\text{upwell}} - F_{\text{den.wc.}} \Delta_{\text{den.wc.}}) / M_{\text{NO}_3^-}$$

The average isotopic rate of change is 14.7‰ , 4.7‰ , and 0.3‰ per 100 m within the shallow water facies of the Bangemall, Roper, and Belt basins respectively. The sedimentation rates between the basins were likely different, but if we assume that they were somewhat comparable, then these isotopic rates of change may reflect primary changes in shallow water nitrate. For the Belt basin $d(\delta_{\text{NO}_3^-})/dt$ is an order of magnitude less than in the Bangemall and Roper basins. In the context of our model, this would have to result from the Belt basin either having a

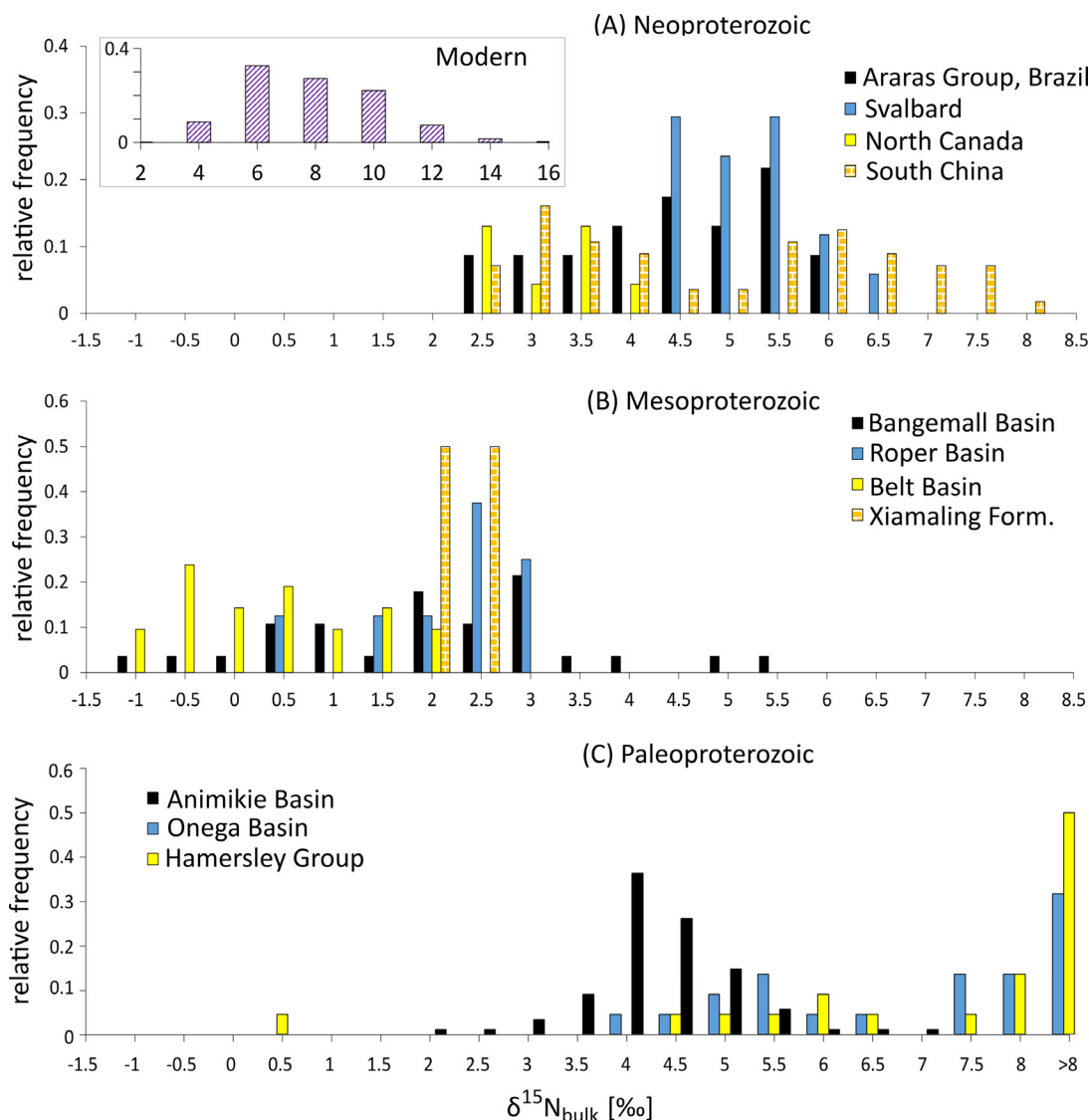


Fig. 6. Histogram of Proterozoic offshore $\delta^{15}\text{N}_{\text{bulk}}$ data. (A) Neoproterozoic era (1.0–0.548 Ga) with data from Ader et al. (2014) and Kikumoto et al. (2014); (B) Mesoproterozoic era (1.6–1.0 Ga) with data from Stüeken (2013), Luo et al. (2015) and this study; (C) Paleoproterozoic era (2.5–1.6 Ga) with data from Busigny et al. (2013), Kump et al. (2011) and Godfrey et al. (2013). Subsets of the datasets listed above were taken to only include offshore environments: from Ader et al. (2014) the Camil, Carmelo, and Copacel sections from Brazil and all data from Svalbard and North Canada. From Kikumoto et al. (2014) all data from the Doushantuo Formation. From Stüeken (2013) data from the Newland Formation in Deep Creek. From the Bangemall and Roper of this study, “deep” and “basinal” data respectively. From Luo et al. (2015) all data. From Busigny et al. (2013) data from the Brockman Iron Formation. From Kump et al. (2011) data from above 180 m in core depth (from 0 m to 180 m). From Godfrey et al. (2013) data from cores MGS-7 and MGS-8. The inset in panel A shows modern marine sediment data from Tesdal et al. (2013). The modern data show no correlation with water depth and are therefore not separated by facies. Paleoproterozoic data from the Aravalli Group (Papineau et al., 2009, 2013) were excluded because they are of higher metamorphic grade and their depositional environment is uncertain.

greater nitrate reservoir in shallow waters ($M_{\text{NO}_3^-}$), or smaller fluxes ($F_{\text{upwell}} \cdot \Delta_{\text{upwell}}$ and $F_{\text{den.wc}} \cdot \Delta_{\text{den.wc}}$). It is unlikely that the Belt basin had a greater nitrate reservoir compared to the Bangemall and Roper basins because it was likely more restricted from the open ocean (see following section). As a result of this restriction, upwelling and water column denitrification fluxes were likely smaller in magnitude in the Belt basin than those in the Bangemall and Roper basins.

In this conceptual model, then, the Bangemall and Roper basins, having a greater connection to the open ocean, had larger upwelling and denitrification fluxes that, when altered, resulted in changes in the isotopic composition of the shallow nitrate reservoir. This variability is reflected in the variability of $\delta^{15}\text{N}_{\text{bulk}}$ values from the shallow water depositional environments in each basin. Variability in the deep basin can be attributed to a small nitrogen reservoir, where incursions of nitrate into the deep

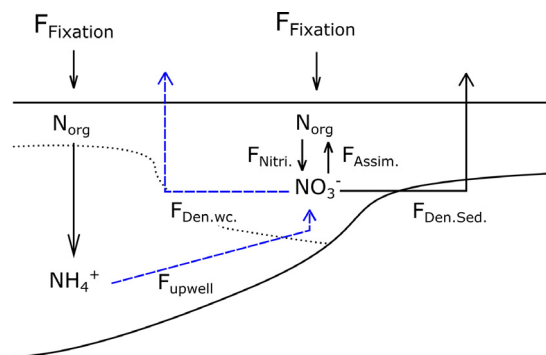


Fig. 7. Schematic of the proposed Mesoproterozoic nitrogen cycle. Shown are fluxes (F) both in and out of a shallow water nitrate reservoir as we propose for the Bangemall and Roper basins. Blue dashed flux arrows represent fluxes that, when varied, are most likely able to change the isotopic composition of a relatively small nitrate reservoir. All other fluxes are unlikely to change the isotopic composition of the nitrate reservoir. Flux labels are as follows: $F_{\text{fixation}} = \text{N}_2$ fixation flux, $F_{\text{nitri.}}$ = nitrification of organic matter to nitrate, $F_{\text{assim.}}$ = assimilation of nitrate into biomass, $F_{\text{den.wc.}}$ = water-column denitrification, $F_{\text{den.sed.}}$ = sedimentary denitrification, F_{upwell} = upwelling of ammonium from anoxic waters. (For interpretation of the references to colour in this figure legend, the reader is referred to the web version of this article.)

ocean could not fully be isotopically buffered by existing NH_4^+ . If the fixed nitrogen reservoir had been larger in the Mesoproterozoic ocean, then it would have been less susceptible to isotopic change. The degree of variability in our sample sets may thus be a reflection of a small and isotopically variable nitrogen supply in comparison to the Paleo- and Neoproterozoic settings that are more uniform in $\delta^{15}\text{N}_{\text{bulk}}$ (Section 5.6).

5.5. Comparing the Bangemall and Roper basins to the Belt basin

The Bangemall and Roper basins show facies-dependent trends in nitrogen isotopes similar in direction to but smaller in magnitude than the Mesoproterozoic Belt Supergroup (Table 3; Stüeken, 2013), suggesting that such a pattern may have been common in the Mesoproterozoic Era. The Belt basin, however, has a deep depositional environment where 80% ($n = 21$) of the samples fall within the range of Nif N_2 fixation, compared to 36% and 8% in the Bangemall and Roper respectively. This difference could be an artifact of sampling, if relatively deeper facies were sampled in the Belt and not captured in the Bangemall transects and Roper samples. However, the Belt basin could instead have been more restricted and consequently more strongly stratified than the Bangemall and Roper basins, which may have led more rapid depletion of the dissolved nitrate reservoir. This hypothesis is supported by the geometry of the Belt basin, which is thought to have been formed by intracontinental rifting (Lydon, 2007) and may only have had limited exchange with the open ocean for some of its history (e.g. Winston, 1990; Luepke and Lyons, 2001; Pratt, 2001). The unusually steep gradient in organic carbon isotopes from -32.2‰ to -22.9‰ , which is not seen in any other

Mesoproterozoic basins (Guo et al., 2013, this study), further supports significant water mass stratification in the Belt basin. Hence the subtler carbon and nitrogen isotopic gradients in the Roper and Bangemall basins may be more representative of global marine conditions. Importantly, none of the three basins show nitrogen isotope values within the range of vanadium or iron-based nitrogenases ($< -6\text{‰}$, Zhang et al., 2014), suggesting that Mo was available in sufficient quantities for the dominance of the molybdenum nitrogenase despite being present at low concentrations in the Mesoproterozoic ocean (Reinhard et al., 2013).

5.6. Mesoproterozoic nitrate minimum

While available data are consistent with a basinal gradient in $\delta^{15}\text{N}_{\text{bulk}}$ and thus in nitrogen speciation in the Mesoproterozoic (Section 5.3), this was not the case in the earlier and later Precambrian. In the mid-Archean Witwatersrand Supergroup (2.87–2.96 Ga), sediments deposited near estuaries ($+1.2 \pm 1.0\text{‰}$) are on average slightly heavier than marine sediments further offshore ($-1.6 \pm 0.8\text{‰}$) (Stüeken et al., 2015a), but almost all of these values fall within the range of biological N_2 fixation. The subtle gradient is thus more likely a result of varying Fe^{2+} availability to diazotrophic microbes (Zerkle et al., 2008) rather than a gradient in nitrate abundance. Nitrate was likely scarce in all parts of the mid-Archean ocean, including shallow waters (Stüeken et al., 2015a), consistent with very low levels of atmospheric oxygen at this time (Pavlov and Kasting, 2002; Kurzweil et al., 2013; Lyons et al., 2014). Surface water nitrate levels may have increased in the late Archean with the onset of low levels of oxidative weathering and enhanced oxygenation of the surface ocean (Siebert et al., 2005; Wille et al., 2007; Kendall et al., 2010; Stüeken et al., 2012; Zerkle et al., 2012; Gregory et al., 2015; Kurzweil et al., 2015). In the Ghaap Group in South Africa (2.67–2.52 Ga), bulk $\delta^{15}\text{N}_{\text{bulk}}$ values have a mean of $+4.6 \pm 2.0\text{‰}$ and show no systematic variation between different facies, which include shallow-water microbialites and deeper-water siliciclastic sediments (Godfrey and Falkowski, 2009). These results were interpreted as evidence of aerobic nitrogen cycling (Godfrey and Falkowski, 2009), implying that nitrate had become a significant ion in the surface ocean at this time. Across the Archean-Proterozoic boundary in the Hamersley Group in Western Australia (2.50–2.46 Ga), combined data sets from Garvin et al. (2009) and Busigny et al. (2013) capture offshore marine facies from the outer shelf and the shelf edge, respectively, and in both settings values are mostly above $+4\text{‰}$, especially after the ‘whiff of oxygen’ at 2.5 Ga (Anbar et al., 2007; Garvin et al., 2009; Stüeken et al., 2015b). Although data from contemporaneous shallow marine sediments are not available, these fairly heavy values in offshore sediments are distinct from the comparatively light values found in the Mesoproterozoic (Stüeken, 2013, this study) and provide strong evidence for a significant reservoir of nitrate throughout the surface ocean at the end of the Archean and extending into the early Paleoproterozoic. From the late Paleoproterozoic, Godfrey et al.

(2013) analyzed drill-core samples along a basinal profile in the Animikie Group (1.87–1.84 Ga) and reported a subtle gradient of 1.0–1.4‰ from onshore to offshore, the latter being slightly lighter, but nearly all their values (98%) were above +3‰ irrespective of environment. Hence nitrate was probably relatively abundant in the surface ocean across all environments in the Animikie basin. This may also have been the case in most of the Neoproterozoic where bulk $\delta^{15}\text{N}$ values are mostly above +2‰ and show no systematic basinal gradient (Ader et al., 2014). From the late Neoproterozoic onwards, nitrate depletion is only reported during temporary anoxic events (e.g. Rau et al., 1987; Sephton et al., 2002; Ohkouchi et al., 2006; Junium and Arthur, 2007; LaPorte et al., 2009; Schoepfer et al., 2012; Wang et al., 2013; Cremonese et al., 2014); throughout most of the Phanerozoic the nitrogen cycle seems to have been predominantly aerobic with little spatial variance (Algeo et al., 2014). Hence the Mesoproterozoic basins analyzed in this study appear to be anomalous in displaying subtle but significant facies-dependent variation in nitrogen isotopes and, by inference, nitrogen speciation.

We cannot rule out the possibility that this pattern is biased by latitudinal or oceanographic effects, because all of the Mesoproterozoic sites were originally located at low latitudes (<30°, Idnurm et al., 1995; Elston et al., 2002) and in epicontinental seas, which could have enhanced stagnation and stratification of the water column. The Paleoproterozoic Animikie basin, on the other hand, formed at a higher latitude (>60°, Symons, 1966) possibly under colder temperatures, which would have favored downward mixing of oxidants produced in the upper ocean. Samples from other localities and better constraints on paleolatitude for other Precambrian basins would be needed to test this possibility.

The relatively light $\delta^{15}\text{N}_{\text{bulk}}$ values in offshore sediments from the Mesoproterozoic are unique and may have been a global characteristic of this time period (Fig. 6). Fig. 1 shows a compilation of bulk nitrogen isotopic compositions from offshore marine environments, highlighting the decline between ~1.7 Ga and ~1.2 Ga or possibly later. This interval post-dates the proposed mid-Paleoproterozoic oxygen overshoot (~2.3–2.0 Ga, Bekker and Holland, 2012; Canfield et al., 2013; Partin et al., 2013; Hardisty et al., 2014) and has recently been identified as a time when atmospheric pO_2 may have dropped back to as little as 0.1% or as great as 4% (Zhang et al., 2016; Cox et al., 2016) of present atmospheric levels until a second, potentially protracted rise to nearer modern amounts across the Neoproterozoic/Paleozoic, possibly beginning at ~800 Ma (Planavsky et al., 2014; Blamey et al., 2016). Statistical analysis of global Fe-speciation data indicates that while subsurface anoxia was widespread throughout the Proterozoic Eon, euxinia was disproportionately common in Mesoproterozoic oceans (Sperling et al., 2015), consistent with lower atmospheric oxygen levels. Marine sulfate concentrations are also thought to have declined after 1.7 Ga from ~10 mM to less than 1.8 mM, followed by a return to >2–3 mM after 1.3 Ga (Kah et al., 2004; Planavsky et al., 2012; Luo et al., 2014; Scott et al., 2014). Given that the redox potential of nitrate is intermediate between that of

sulfate and oxygen (Brookins, 1988), it is plausible that the abundance of nitrate in the surface ocean also declined in the mid-Proterozoic. This would have encouraged microbial N_2 fixation, leading to relatively low $\delta^{15}\text{N}_{\text{bulk}}$ values in offshore marine sediments (Fig. 6). Nitrification of ammonium to nitrate requires oxygen, and so the production of nitrate was perhaps favored in shallow waters where O_2 was actively being produced. In contrast, nitrification may have been suppressed further offshore where O_2 production was lower.

5.7. Implications for life

Both the Bangemall and the Roper basins have fossil assemblages that are consistent with an onshore-offshore trend of decreasing organismic diversity and abundance seawards (Buick and Knoll, 1999; Javaux et al., 2001). Stüeken (2013) suggested there could be a linkage between the basinal nitrate gradient observed in the Belt basin and the fossil distributions in the Bangemall and Roper basins, if they also had a nitrate gradient. Although our data are inconsistent with complete nitrate depletion offshore in the Roper and Bangemall basins (unlike in the Belt basin), several features of our results indicate that nitrate concentrations were probably significantly lower than in the Paleoproterozoic, Neoproterozoic, and modern ocean. First, $\delta^{15}\text{N}$ values were below +3‰ in offshore Mesoproterozoic sediments compared to +4‰ to +5‰ in the Cenozoic and modern (Tesdal et al., 2013; Algeo et al., 2014) (Fig. 6), which likely reflects a mixture of two biological inputs from nitrate-assimilating organisms ($\delta^{15}\text{N} > 0‰$) and diazotrophs ($\delta^{15}\text{N} \sim 0‰$). The latter would not have been ecologically significant if nitrate had been abundant because N_2 fixation is energetically costly. Second, the lightest $\delta^{15}\text{N}_{\text{bulk}}$ data from the peritidal facies suggest rapid nitrate depletion and domination by N_2 fixers during temporary restriction from the marine nitrate reservoir. This is consistent with microfossil evidence from the Bangemall basin peritidal facies where *Palaeopleurocapsa*, which resembles a modern genus of nitrogen-fixing cyanobacteria (Section 2.1), has been reported (Buick and Knoll, 1999). Further support comes from biomarker evidence from the late Mesoproterozoic Taoudeni basin (1.1 Ga), which indicates that even some shallow waters during the Mesoproterozoic could have also been deficient in oxidized nitrogen species (Blumenberg et al., 2012). Lastly, the variability in $\delta^{15}\text{N}$ throughout the basins is best explained by a small nitrate reservoir whose relative size and isotopic composition were easily perturbed. Similar variability is seen in sulfur isotopes from the Mesoproterozoic, which is interpreted as an artifact of a small sulfate reservoir (Kah et al., 2004; Guo et al., 2015). It is likely that the magnitude of nitrogen speciation trends varied between different basins; nevertheless all the currently available nitrogen isotope data point towards generally low Mesoproterozoic nitrate concentrations in the surface ocean with a minimum in offshore waters.

If so, then nitrogen availability may have contributed to the ecological distribution of marine organisms. As photosynthetic eukaryotes are apparently outcompeted by

prokaryotes in nitrate-limited environments (Malone, 1980; Li et al., 1992; Lindell and Post, 1995; Latasa and Bidigare, 1998; Karl et al., 2001; Bouman et al., 2011; Fawcett et al., 2011), it is likely that the open ocean was dominated by prokaryotic organisms with eukaryotes perhaps only inhabiting the most oxygenated part of the water column. Nearer shore, a more diverse ecosystem including abundant eukaryotes may have developed in relatively nitrate-rich waters. The very shallowest peritidal settings may again have excluded eukaryotes, not because of anoxia but due to periodic nitrate depletion during intervals of restricted water exchange at low tides. This ecological gradient may have also had evolutionary consequences in that eukaryote diversification was not possible in offshore and onshore nitrate-poor settings but was instead confined to near-shore waters that were relatively nitrate-rich. It is also possible that eukaryotic life was inhibited directly by episodic upwelling of anoxic and sometimes sulfidic waters (Johnston et al., 2009); these two mechanisms of eukaryotic inhibition are not mutually exclusive and likely both occurred. If so, then perhaps eukaryotes underwent a major evolutionary radiation and rise to ecological dominance only after a Neoproterozoic oxygen increase, resulting in globally prevalent nitrification and deeper or less widespread anoxic water masses. Thus, our data support the hypothesis of Anbar and Knoll (2002) that nitrogen availability may have been a key constraint on the evolution of eukaryotes.

6. CONCLUSION

Nitrogen isotope data from the Bangemall and Roper basins, considered in concert with the Belt basin (Stüeken, 2013), are consistent with the idea that distinct facies-dependent nitrogen regimes (largely aerobic near-shore and partially to fully anaerobic offshore) were a common feature in the early Mesoproterozoic. Peak enrichment in $\delta^{15}\text{N}_{\text{bulk}}$ occurs in shallow depositional environments and cannot solely be explained by post-depositional alteration. There is no apparent systematic cross-basin bias of oxic versus anoxic diagenesis or metamorphism, so it is likely that these heavy values reflect the primary isotopic composition of biomass forming in the water column. The most plausible explanation for positive $\delta^{15}\text{N}_{\text{bulk}}$ values in the shallower waters is that a pool of dissolved nitrate was partially denitrified and the residual isotopically heavy nitrate was subsequently assimilated into biomass, as in the modern ocean (e.g. Sigman et al., 2009a). Instances of light $\delta^{15}\text{N}_{\text{bulk}}$ in peritidal environments probably represent transient periods of isolation from the marine nitrate supply at low tide leaving fixation as the primary source of nitrogen. Light $\delta^{15}\text{N}_{\text{bulk}}$ values in deep water samples are consistent with a predominance of N_2 fixation by the Mo-Fe nitrogenase; slightly heavier samples likely record mixing with biomass from nitrate assimilators during intervals when nitrate was more available in the surface ocean, as in parts of the modern redox-stratified Cariaco basin (Montes et al., 2013). Such mixing implies that nitrate concentrations were low, because any isotopic signal from N_2 fixation would be erased without a nitrate deficit in the water column (e.g. Fulton et al., 2012).

It is not clear whether the proposed spatial and temporal trends in nitrogen cycling indicate reduced concentrations of trace metals, oxygen, or both in deep water environments during the Mesoproterozoic where aerobic nitrogen cycling seems to have been limited. Our results are consistent with metal-nitrogen co-limitation controlled by the extent of euxinic conditions (Anbar and Knoll, 2002; Glass et al., 2009; Reinhard et al., 2013), but probably only to a degree that it limited nitrification and denitrification offshore while N_2 -fixation by the Mo-Fe nitrogenase was able to persist. Our data are also consistent with a Mesoproterozoic oxygen decline (Bekker and Holland, 2012; Planavsky et al., 2012; Partin et al., 2013; Scott et al., 2014), as nitrogen isotopic ratios are lower in the Mesoproterozoic than in the Paleo- and Neoproterozoic, suggesting relatively lower nitrate concentrations. A basal gradient of dissolved oxygen concentrations (higher near-shore to lower offshore) could potentially also produce the nitrogen isotopic trend seen in our datasets by limiting the extent of nitrification. Thus the theoretical prediction of two spatially separated states of the nitrogen cycle in the mid-Proterozoic (Boyle et al., 2013) is now expressed in three different Mesoproterozoic basins, though how much this pattern directly depended on the location and extent of underlying euxinic waters is still unclear. Regardless, such patterns would probably have restricted eukaryote biomass and evolution to near-shore settings, as hypothesized by Anbar and Knoll (2002), though the key limiting factor may not have been nitrogen fixation rates but nitrogen speciation.

ACKNOWLEDGEMENTS

We thank NSF EAR FESD grant #1338810 (RB), NASA grant NNX16AI37G (RB), the Agouron Institute (RB), the NASA Astrobiology Institute's Virtual Planetary Laboratory (RB), the NSF Graduate Research Fellowship Program (MAK), and the Department of Earth and Space Sciences, University of Washington Goodspeed Geology Fellowship (MCK), Misch Fellowship (MCK), and the Kenneth C. Robbins Field Study Fellowship (2014, MCK) for funding, Andrew Schauer, Virginia Littell, and the University of Washington Isolab for technical support, and Simon Poulton for three additional Roper Group samples. We also thank Chris Reinhard and two anonymous reviewers and the associate editor James Farquhar for their comments that significantly improved this paper.

REFERENCES

- Abbott S. T. and Sweet I. P. (2000) Tectonic control on third-order sequences in a siliciclastic ramp-style basin: an example from the Roper Superbasin (Mesoproterozoic), northern Australia. *Aust. J. Earth Sci.* **47**, 637–657.
- Ader M., Sansjofre P., Halverson G. P., Busigny V., Trindade R. I., Kunzmann M. and Nogueira A. C. (2014) Ocean redox structure across the Late Neoproterozoic oxygenation event: a nitrogen isotope perspective. *Earth Planet. Sci. Lett.* **396**, 1–13.
- Ader M., Thomazo C., Sansjofre P., Busigny V., Papineau D., Laffont R., Cartigny P. and Halverson G. P. (2016) Interpretation of the nitrogen isotopic composition of Precambrian sedimentary rocks: assumptions and perspectives. *Chem. Geol.* **429**, 93–110.

- Algeo T. J., Meyers P. A., Robinson R. S., Rowe H. and Jiang G. Q. (2014) Icehouse-greenhouse variations in marine denitrification. *Biogeosciences* **11**, 1273–1295.
- Altabet M. A. and Francois R. (1994) Sedimentary nitrogen isotopic ratio as a recorder for surface ocean nitrate utilization. *Global Biogeochem. Cycles* **8**, 103–116.
- Anbar A. D. and Knoll A. H. (2002) Proterozoic ocean chemistry and evolution: a bioinorganic bridge? *Science* **297**, 1137–1142.
- Anbar A., Duan Y., Lyons T. W., Arnold G. L., Kendall B., Creaser R. A., Kaufman A. J., Gordon G. W., Scott C. T., Garvin J. and Buick R. (2007) A whiff of oxygen before the Great Oxidation Event? *Science* **317**, 1903–1906.
- Arnold G. L., Anbar A. D., Barling J. and Lyons T. W. (2004) Molybdenum isotope evidence for widespread anoxia in mid-Proterozoic oceans. *Science* **304**, 87–90.
- Bartley J. K. and Kah L. C. (2004) Marine carbon reservoir, C_{org} - C_{carb} coupling, and the evolution of the Proterozoic carbon cycle. *Geology* **32**, 129–132.
- Bebout G. E. and Fogel M. L. (1992) Nitrogen-isotopic composition of metasedimentary rocks in the Catalina Schist, California: implications for metamorphic devolatilization history. *Geochim. Cosmochim. Acta* **56**, 2839–2849.
- Bekker A. and Holland H. D. (2012) Oxygen overshoot and recovery during the early Paleoproterozoic. *Earth Planet. Sci. Lett.* **317**, 295–304.
- Bekker A., Holland H. D., Wang P.-L., Rumble, III, D., Stein H. J., Hannah J. L., Coetzee L. L. and Beukes N. J. (2004) Dating the rise of atmospheric oxygen. *Nature* **427**, 117–120.
- Bekker A., Holmden C., Beukes N. J., Kenig F., Eglinton B. and Patterson W. P. (2008) Fractionation between inorganic and organic carbon during the Lomagundi (2.22–2.1 Ga) carbon isotope excursion. *Earth Planet. Sci. Lett.* **271**, 278–291.
- Blamey N. J. F., Brand U., Parnell J., Spear N., Lécuyer C., Benish K., Meng F. and Ni P. (2016) Paradigm shift in determining Neoproterozoic atmospheric oxygen. *Geology* **44**, 651–654.
- Blumenberg M., Thiel V., Riegel W., Kah L. C. and Reitner J. (2012) Biomarkers of black shales formed by microbial mats, Late Mesoproterozoic (1.1 Ga) Taoudeni Basin, Mauritania. *Precambrian Res.* **196**, 113–127.
- Bouman H. A., Ulloa O., Barlow R., Li W. K., Platt T., Zwirgmaier K., Scanlan D. J. and Sathyendranath S. (2011) Water-column stratification governs the community structure of subtropical marine picophytoplankton. *Environ. Microbiol. Rep.* **3**, 473–482.
- Boyle R. A., Clark J. R., Poulton S. W., Shields-Zhou G., Canfield D. E. and Lenton T. M. (2013) Nitrogen cycle feedbacks as a control on euxinia in the mid-Proterozoic ocean. *Nat. Commun.* **4**. <http://dx.doi.org/10.1038/ncomms2511>.
- Brookins D. G. (1988) *Eh-pH Diagrams for Geochemistry*. Springer-Verlag, New York.
- Brunner B., Contreras S., Lehmann M. F., Matantseva O., Rollog M., Kalvelage T., Klockgether G., Lavik G., Jetten M. S. M., Kartal B. and Kuypers M. M. (2013) Nitrogen isotope effects induced by anammox bacteria. *Proc. Natl. Acad. Sci.* **110**, 18994–18999.
- Buick R. (2007) Did the Proterozoic 'Canfield Ocean' cause a laughing gas greenhouse? *Geobiology* **5**, 97–100.
- Buick R. and Knoll A. H. (1999) Acritarchs and microfossils from the Mesoproterozoic Bangemall Group, northwestern Australia. *J. Paleontol.* **73**, 744–764.
- Buick R., Des Marais D. J. and Knoll A. H. (1995) Stable isotopic compositions of carbonates from the Mesoproterozoic Bangemall Group, northwestern Australia. *Chem. Geol.* **123**, 153–171.
- Busigny V., Lebeau O., Ader M., Krapež B. and Bekker A. (2013) Nitrogen cycle in the Late Archean ferruginous ocean. *Chem. Geol.* **362**, 115–130.
- Canfield D. E. (1998) A new model for Proterozoic ocean chemistry. *Nature* **396**, 450–453.
- Canfield D. E. and Teske A. (1996) Late Proterozoic rise in atmospheric oxygen concentration inferred from phylogenetic and sulphur-isotope studies. *Nature* **382**, 127–132.
- Canfield D. E., Ngombi-Pemba L., Hammarlund E. U., Bengtson S., Chaussidon M., Gauthier-Lafaye F., Meunier A., Riboulleau A., Rollion-Bard C., Rouxel O., Asael D., Pierson-Wickmann A.-C. and El Albani A. (2013) Oxygen dynamics in the aftermath of the Great Oxidation of Earth's atmosphere. *Proc. Natl. Acad. Sci.* **110**, 16736–16741.
- Casciotti K. L. (2009) Inverse kinetic isotope fractionation during bacterial nitrite oxidation. *Geochim. Cosmochim. Acta* **73**, 2061–2076.
- Cox G. M., Jarrett A., Edwards D., Crockford P. W., Halverson G. P., Collins A. S., Poirier A. and Li Z. X. (2016) Basin redox and primary productivity within the Mesoproterozoic Roper Seaway. *Chem. Geol.* **440**, 101–114.
- Cremonese L., Shields-Zhou G. A., Struck U., Ling H. F. and Och L. M. (2014) Nitrogen and organic carbon isotope stratigraphy of the Yangtze Platform during the Ediacaran-Cambrian transition in South China. *Palaeogeogr. Palaeoclimatol. Palaeoecol.* **398**, 165–186.
- Czaja A. D., Johnson C. M., Beard B. L., Eigenbrode J. L., Freeman K. H. and Yamaguchi K. E. (2010) Iron and carbon isotope evidence for ecosystem and environmental diversity in the ~2.7 to 2.5 Ga Hamersley Province, Western Australia. *Earth Planet. Sci. Lett.* **292**, 170–180.
- Donnelly T. H. and Crick I. H. (1988) Depositional environment of the middle Proterozoic Velkerri Formation in northern Australia: geochemical evidence. *Precamb. Res.* **42**, 165–172.
- Dutkiewicz A., Volk H., Ridley J. and George S. (2003) Biomarkers, brines, and oil in the Mesoproterozoic, Roper Superbasin, Australia. *Geology* **31**, 981–984.
- Dutkiewicz A., Volk H., Ridley J. and George S. C. (2004) Geochemistry of oil in fluid inclusions in a middle Proterozoic igneous intrusion: implications for the source of hydrocarbons in crystalline rocks. *Org. Geochem.* **35**, 937–957.
- Eigenbrode J. L. and Freeman K. H. (2006) Late Archean rise of aerobic microbial ecosystems. *Proc. Natl. Acad. Sci.* **103**, 15759–15764.
- Elston D. P., Enkin R. J., Baker J. and Kisilevsky D. K. (2002) Tightening the Belt: paleomagnetic-stratigraphic constraints on deposition, correlation, and deformation of the Middle Proterozoic (ca. 1.4 Ga) Belt-Purcell Supergroup, United States and Canada. *Geol. Soc. Am. Bull.* **114**, 619–638.
- Farquhar J., Zerkle A. L. and Bekker A. (2011) Geological constraints on the origin of oxygenic photosynthesis. *Photosynth. Res.* **107**, 11–36.
- Fawcett S. E., Lomas M. W., Casey J. R., Ward B. B. and Sigman D. M. (2011) Assimilation of upwelled nitrate by small eukaryotes in the Sargasso Sea. *Nat. Geosci.* **4**, 717–722.
- Flannery E. N. and George S. C. (2014) Assessing the syngeneity and indigeneity of hydrocarbons in the ~1.4 Ga Velkerri Formation, McArthur Basin, using slice experiments. *Org. Geochem.* **77**, 115–125.
- Freude C. and Blaser M. (2016) Carbon isotope fractionation during catabolism and anabolism in acetogenic bacteria growing on different substrates. *Appl. Environ. Microbiol.* **82**, 2728–2737.
- Freudenthal T., Wagner T., Wenzhoefer F., Zabel M. and Wefer G. (2001) Early diagenesis of organic matter from sediments of the eastern subtropical Atlantic: evidence from stable nitrogen and carbon isotopes. *Geochim. Cosmochim. Acta* **65**, 1795–1808.
- Frey C., Hietanen S., Jürgens K., Labrenz M. and Voss M. (2014) N and O isotope fractionation in nitrate during chemolithoau-

- trophic denitrification by *Sulfurimonas gotlandica*. *Environ. Sci. Technol.* **48**, 13229–13237.
- Fuchsman C. A., Murray J. K. and Kononov S. K. (2008) Concentration and natural stable isotope profiles of nitrogen species in the Black Sea. *Marine Chem.* **111**, 90–105.
- Füssel J., Lam P., Lavik G., Jensen M. M., Holtappels M., Günter M. and Kuypers M. M. M. (2012) Nitrite oxidation in the Namibian oxygen minimum zone. *ISME J.* **6**, 1200–1209.
- Fulton J. M., Arthur M. A. and Freeman K. H. (2012) Black Sea nitrogen cycling and the preservation of phytoplankton $\delta^{15}\text{N}$ signals during the Holocene. *Global Biogeochem. Cycles* **26**. <http://dx.doi.org/10.1029/2011GB004196>.
- Galbraith E., Kienast M. and NICOPP (2013) The acceleration of oceanic denitrification during deglacial warming. *Nat. Geosci.* **6**, 579–584.
- Garvin J., Buick R., Anbar A. D., Arnold G. L. and Kaufman A. J. (2009) Isotopic evidence for an aerobic nitrogen cycle in the latest Archean. *Science* **323**, 1045–1048.
- Gilleaudeau G. J. and Kah L. C. (2013) Carbon isotope records in a Mesoproterozoic epicratonic sea: carbon cycling in a low-oxygen world. *Precamb. Res.* **228**, 85–101.
- Glass J. B., Wolfe-Simon F. and Anbar A. D. (2009) Coevolution of metal availability and nitrogen assimilation in cyanobacteria and algae. *Geobiology* **7**, 100–123.
- Glass J. B., Axler R. P., Chandra S. and Goldman C. R. (2012) Molybdenum limitation of microbial nitrogen assimilation in aquatic ecosystems and pure cultures. *Front. Microbiol.* **3**. <http://dx.doi.org/10.3389/fmicb.2012.00331>.
- Godfrey L. V. and Falkowski P. G. (2009) The cycling and redox state of nitrogen in the Archean ocean. *Nat. Geosci.* **2**, 725–729.
- Godfrey L. V. and Glass J. B. (2011) The geochemical record of the ancient nitrogen cycle, nitrogen isotopes, and metal cofactors. *Methods Enzymol.* **486**, 483–506.
- Godfrey L. V., Poulton S. W., Bebout G. E. and Fralick P. W. (2013) Stability of the nitrogen cycle during development of sulfidic water in the redox-stratified late Paleoproterozoic ocean. *Geology* **41**, 655–658.
- Granger J., Prokopenko M. G., Sigman D. M., Mordy C. W., Morse Z. M., Morales L. V., Sambrotto R. N. and Plessen B. (2011) Coupled nitrification-denitrification in sediment of the eastern Bering Sea shelf leads to ^{15}N enrichment of fixed N in shelf waters. *J. Geophys. Res.: Oceans* **116**. <http://dx.doi.org/10.1029/2010JC006751>.
- Gregory D. D., Large R. R., Halpin J. A., Steadman J. A., Hickman A. H., Ireland T. R. and Holden P. (2015) The chemical conditions of the late Archean Hamersley basin inferred from whole rock and pyrite geochemistry with $\Delta^{33}\text{S}$ and $\delta^{34}\text{S}$ isotope analyses. *Geochim. Cosmochim. Acta* **149**, 223–250.
- Guo H., Du Y., Kah L. C., Huang J., Hu C., Huang H. and Yu W. (2013) Isotopic composition of organic and inorganic carbon from the Mesoproterozoic Jixian Group, North China: implications for biological and oceanic evolution. *Precamb. Res.* **224**, 169–183.
- Guo H., Du Y., Kah L. C., Hu C., Huang J., Huang H., Yu W. and Song H. (2015) Sulfur isotope composition of carbonate-associated sulfate from the Mesoproterozoic Jixian Group, North China: implications for the marine sulfur cycle. *Precamb. Res.* **266**, 319–336.
- Haendel D., Muehle K., Nitzsche H.-M., Stiehl G. and Wand U. (1986) Isotopic variations of the fixed nitrogen in metamorphic rocks. *Geochim. Cosmochim. Acta* **50**, 749–758.
- Hardisty D. S., Lu Z., Planavsky N. J., Bekker A., Philippot P., Zhou X. and Lyons T. W. (2014) An iodine record of Paleoproterozoic surface ocean oxygenation. *Geology* **42**, 619–622.
- Haug G. H., Pedersen T. F., Sigman D. M., Calvert S. E., Nielsen B. and Peterson L. C. (1998) Glacial/interglacial variations in production and nitrogen fixation in the Cariaco Basin during the last 580 kyr. *Paleoceanography* **13**, 427–432.
- Hayes J. M. (2001) Fractionation of carbon and hydrogen isotopes in biosynthetic processes. *Rev. Mineral. Geochem.* **43**, 225–277.
- Hayes J. M., Kaplan I. R. and Wedeking K. W. (1983) Precambrian organic geochemistry, preservation of the record. In *Earth's earliest biosphere – its origin and evolution* (ed. J. W. Schopf). Princeton University Press, Princeton, NJ, pp. 93–134.
- Hoefs J. and Frey M. (1976) The isotopic composition of carbonaceous matter in a metamorphic profile from the Swiss Alps. *Geochim. Cosmochim. Acta* **40**, 945–951.
- Idnurm M., Giddings J. W. and Plumb K. A. (1995) Apparent polar wander and reversal stratigraphy of the Palaeo-Mesoproterozoic southeastern McArthur Basin, Australia. *Precamb. Res.* **72**, 1–41.
- Jackson M. J. and Raiswell R. (1991) Sedimentology and carbon-sulphur geochemistry of the Velkerri Formation, a mid-Proterozoic potential oil source in northern Australia. *Precamb. Res.* **54**, 81–108.
- Jackson M. J., Sweet I. P. and Powell T. G. (1988) Studies on Petroleum geology and geochemistry, Middle Proterozoic, McArthur Basin, northern Australia: I. Petroleum potential. *APEA J.* **28**, 283–302.
- Javaux E. J., Knoll A. H. and Walter M. R. (2001) Morphological and ecological complexity in early eukaryotic ecosystems. *Nature* **412**, 66–69.
- Javaux E. J., Knoll A. H. and Walter M. R. (2004) TEM evidence for eukaryotic diversity in mid-Proterozoic oceans. *Geobiology* **2**, 121–132.
- Jia Y. (2006) Nitrogen isotope fractionations during progressive metamorphism: a case study from the Paleozoic Cooma metasedimentary complex, southeastern Australia. *Geochim. Cosmochim. Acta* **70**, 5201–5214.
- Johnston D. T., Farquhar J., Summons R. E., Shen Y., Kaufman A. J., Masterson A. L. and Canfield D. E. (2008) Sulfur isotope biogeochemistry of the Proterozoic McArthur Basin. *Geochim. Cosmochim. Acta* **72**, 4278–4290.
- Johnston D. T., Wolfe-Simon F., Pearson A. and Knoll A. H. (2009) Anoxygenic photosynthesis modulated Proterozoic oxygen and sustained Earth's middle age. *Proc. Natl. Acad. Sci.* **106**, 16925–16929.
- Junium C. K. and Arthur M. A. (2007) Nitrogen cycling during the Cretaceous, Cenomanian-Turonian Oceanic Anoxic Event II. *Geochim. Geophys. Geosyst.* **8**. <http://dx.doi.org/10.1029/2006GC001328>.
- Kah L. C., Lyons T. W. and Frank T. D. (2004) Low marine sulphate and protracted oxygenation of the Proterozoic biosphere. *Nature* **431**, 834–838.
- Karl D. M., Bidigare R. R. and Letelier R. M. (2001) Long-term changes in plankton community structure and productivity in the North Pacific Subtropical Gyre: the domain shift hypothesis. *Deep Sea Res. Part II* **48**, 1449–1470.
- Kendall B., Creaser R. A., Gordon G. W. and Anbar A. (2009) Re-Os and Mo isotope systematics of black shales from the middle Proterozoic Velkerri and Wollongoran formations, McArthur basin, northern Australia. *Geochim. Cosmochim. Acta* **73**, 2534–2558.
- Kendall B., Reinhard C. T., Lyons T. W., Kaufman A. J., Poulton S. W. and Anbar A. (2010) Pervasive oxygenation along late Archean ocean margins. *Nat. Geosci.* **3**, 647–652.
- Kessler A. J., Bristow L. A., Cardenas M. B., Glud R. N., Thamdrup B. and Cook P. L. (2014) The isotope effect of denitrification in permeable sediments. *Geochim. Cosmochim. Acta* **133**, 156–167.

- Kikumoto R., Tahata M., Nishizawa M., Sawaki Y., Maruyama S., Shu D., Han J., Komiya T., Takai K. and Ueno Y. (2014) Nitrogen isotope chemostratigraphy of the Ediacaran and Early Cambrian platform sequence at Three Gorges, South China. *Gondwana Res.* **25**, 1057–1069.
- Kralik M. (1982) Rb-Sb age determinations on Precambrian carbonate rocks of the Carpentarian McArthur basin, Northern Territories, Australia. *Precamb. Res.* **18**, 157–170.
- Kump L. R., Junium C., Arthur M. A., Brasier A., Fallick A., Melezhik V., Lepland A., CČrne A. E. and Luo G. (2011) Isotopic evidence for massive oxidation of organic matter following the Great Oxidation Event. *Science* **334**, 1694–1696.
- Kurzweil F., Claire M. W., Thomazo C., Peters M., Hannington M. and Strauss H. (2013) Atmospheric sulfur rearrangement 2.7 billion years ago: evidence for oxygenic photosynthesis. *Earth Planet. Sci. Lett.* **366**, 17–26.
- Lalonde S. V. and Konhauser K. O. (2015) Benthic perspective on Earth's oldest evidence for oxygenic photosynthesis. *Proc. Natl. Acad. Sci.* **112**, 995–1000.
- Kurzweil F., Wille M., Schoenberg R., Taubald H. and van Kranendonk M. J. (2015) Continuously increasing $\delta^{98}\text{Mo}$ values in Neoproterozoic black shales and iron formations from the Hamersley Basin. *Geochim. Cosmochim. Acta* **164**, 523–542.
- LaPorte D. F., Holmden C., Patterson W. P., Loxton J. D., Melchin M. J., Mitchell C. E., Finney S. C. and Sheets H. D. (2009) Local and global perspectives on carbon and nitrogen cycling during the Hirnantian glaciation. *Palaeogeogr. Palaeoclimatol. Palaeoecol.* **276**, 182–195.
- Latasa M. and Bidigare R. R. (1998) A comparison of phytoplankton populations of the Arabian Sea during the Spring Intermonsoon and Southwest Monsoon of 1995 as described by HPLC-analyzed pigments. *Deep Sea Res. Part II* **45**, 2133–2170.
- Lehman M. R., Bernasconi S. M., Barbieri A. and McKenzie J. A. (2002) Preservation of organic matter and alteration of its carbon and nitrogen isotope composition during simulated and in situ early sedimentary diagenesis. *Geochim. Cosmochim. Acta* **66**, 3573–3584.
- Li W. K. W., Dickie P. M., Irwin B. D. and Wood A. M. (1992) Biomass of bacteria, cyanobacteria, prochlorophytes and photosynthetic eukaryotes in the Sargasso Sea. *Deep Sea Res. Part A. Oceanograph. Res. Pap.* **39**, 501–519.
- Lindell D. and Post A. F. (1995) Ultraphytoplankton succession is triggered by deep winter mixing in the Gulf of Aqaba (Eilat), Red Sea. *Limnol. Oceanogr.* **40**, 1130–1141.
- Luepke J. J. and Lyons T. W. (2001) Pre-Rodinian (Mesoproterozoic) supercontinental rifting along the western margin of Laurentia: geochemical evidence from the Belt-Purcell Supergroup. *Precamb. Res.* **111**, 79–90.
- Luo G., Ono S., Huang J., Algeo T. J., Li C., Zhou L., Robinson A., Lyons T. W. and Xie S. (2014) Decline in oceanic sulfate levels during the early Mesoproterozoic. *Precamb. Res.* **258**, 36–47.
- Luo G., Hallmann C., Xie S., Ruan X. and Summons R. E. (2015) Comparative microbial diversity and redox environments of black shale and stromatolite facies in the Mesoproterozoic Xiamaling Formation. *Geochim. Cosmochim. Acta* **151**, 150–167.
- Lydon J. W. (2007) Geology and metallogeny of the Belt-Purcell basin. In *Mineral deposits of Canada: a synthesis of major deposit-types, district metallogeny, the evolution of geological provinces, and exploration methods* (ed. W. D. Goodfellow). Geological Association of Canada, Mineral Deposits Division, Special Publication, pp. 581–607.
- Lyons T. W., Reinhard C. T. and Planavsky N. J. (2014) The rise of oxygen in Earth's early ocean and atmosphere. *Nature* **506**, 307–315.
- Macko S. A. and Estep M. L. (1984) Microbial alteration of stable nitrogen and carbon isotopic compositions of organic matter. *Org. Geochem.* **6**, 787–790.
- Macko S. A., Fogel M. L., Hare P. E. and Hoering T. C. (1987) Isotopic fractionation of nitrogen and carbon in the synthesis of amino acids by microorganisms. *Chem. Geol.* **65**, 79–92.
- Martens-Habbena W., Berube P. M., Urakawa H., de la Torre J. R. and Stahl D. A. (2009) Ammonia oxidation kinetics determine niche separation of nitrifying Archaea and Bacteria. *Nature* **461**, 976–979.
- Malone T. C. (1980) Size-fractionated primary productivity of marine phytoplankton. In *Primary productivity in the sea* (ed. P. G. Falkowski). Springer, US, pp. 301–319.
- Martin D. M. (2002) Peperite in the Backdoor Formation and its significance to the age and tectonic evolution of the Bangemall Supergroup. *Western Austr. Geol. Surv. Ann. Rev.* **2002**, 53–59.
- Martin D. M. and Thorne A. M. (2004) Tectonic setting and basin evolution of the Bangemall Supergroup in the northwestern Capricorn Orogen. *Precamb. Res.* **128**, 385–409.
- Martin D. M., Sircombe K. N., Thorne A. M., Cawood P. A. and Nemchin A. A. (2008) Provenance history of the Bangemall Supergroup and implications for the Mesoproterozoic paleogeography of the West Australian Craton. *Precamb. Res.* **166**, 93–110.
- McKirdy D. M. and Powell T. G. (1974) Metamorphic alteration of carbon isotopic composition in ancient sedimentary organic matter: new evidence from Australia and South Africa. *Geology* **2**, 591–595.
- Montes E., Thunell R., Muller-Karger F. E., Lorenzoni L., Tappa E., Troccoli L., Astor Y. and Varela R. (2013) Sources of $\delta^{15}\text{N}$ variability in sinking particulate nitrogen in the Cariaco Basin, Venezuela. *Deep Sea Res. Part II* **93**, 96–107.
- Morales L. V., Granger J., Chang B. X., Prokopenko M. G., Plessen B., Gradinger R. and Sigman D. M. (2014) Elevated $^{15}\text{N}/^{14}\text{N}$ in particulate organic matter, zooplankton, and diatom frustule-bound nitrogen in the ice-covered water column of the Bering Sea eastern shelf. *Deep Sea Res. Part II* **109**, 100–111.
- Nishizawa M., Miyazaki J., Makabe A., Koba K. and Takai K. (2014) Physiological and isotopic characteristics of nitrogen fixation by hyperthermophilic methanogens: key insights into nitrogen anabolism of the microbial communities in Archean hydrothermal systems. *Geochim. Cosmochim. Acta* **138**, 117–135.
- Ohkouchi N., Kashiyama Y., Kuroda J., Ogawa N. O. and Kitazato H. (2006) The importance of diazotrophic cyanobacteria as primary producers during Cretaceous Oceanic Anoxic Event 2. *Biogeosciences* **3**, 467–478.
- Olson S. L., Kump L. R. and Kasting J. F. (2013) Quantifying the areal extent and dissolved oxygen concentrations of Archean oxygen oases. *Chem. Geol.* **362**, 35–43.
- Page R. W., Jackson M. J. and Krassay A. A. (2000) Constraining sequence stratigraphy in north Australian basins: SHRIMP U-Pb zircon geochronology between Mt Isa and McArthur River. *Aust. J. Earth Sci.* **47**, 431–459.
- Papineau D., Purohit R., Goldberg T., Pi D., Shields G. A., Bhu H., Steele A. and Fogel M. L. (2009) High primary productivity and nitrogen cycling after the Paleoproterozoic phosphogenic event in the Aravalli Supergroup, India. *Precamb. Res.* **171**, 37–56.
- Papineau D., Purohit R., Fogel M. L. and Shields-Zhou G. A. (2013) High phosphate availability as a possible cause for massive cyanobacterial production of oxygen in the Paleoproterozoic atmosphere. *Earth Planet. Sci. Lett.* **362**, 225–236.
- Partin C. A., Lalonde S. V., Planavsky N. J., Bekker A., Rouxel O. J., Lyons T. W. and Konhauser K. O. (2013) Uranium in iron

- formations and the rise of atmospheric oxygen. *Chem. Geol.* **362**, 82–90.
- Pavlov A. A. and Kasting J. F. (2002) Mass-independent fractionation of sulfur isotopes in Archean sediments: strong evidence for an anoxic Archean atmosphere. *Astrobiology* **2**, 27–41.
- Peat C. J., Muir M. D., Plumb K. A., McKirdy D. M. and Norvick M. S. (1978) Proterozoic microfossils from the Roper Group, Northern Territory, Australia. *BMR J. Aust. Geol. Geophys.* **3**, 1–17.
- Planavsky N. J., McGoldrick P., Scott C. T., Li C., Reinhard C. T., Kelly A. E., Chu X., Bekker A., Love G. D. and Lyons T. W. (2011) Widespread iron-rich conditions in the mid-Proterozoic ocean. *Nature* **477**, 448–451.
- Planavsky N. J., Bekker A., Hofmann A., Owens J. D. and Lyons T. W. (2012) Sulfur record of rising and falling marine oxygen and sulfate levels during the Lomagundi event. *Proc. Natl. Acad. Sci.* **109**, 18300–18305.
- Planavsky N. J., Reinhard C. T., Wang X., Thomson D., McGoldrick P., Rainbird R. H., Johnson T., Fischer W. W. and Lyons T. W. (2014) Low Mid-Proterozoic atmospheric oxygen levels and the delayed rise of animals. *Science* **346**, 635–638.
- Poulin F. J. and Franks P. J. S. (2010) Size-structured planktonic ecosystems: constraints, controls and assembly instructions. *J. Plankton Res.* **32**, 1121–1130.
- Poulton S. W. and Canfield D. E. (2011) Ferruginous conditions: a dominant feature of the ocean through Earth's history. *Elements* **7**, 107–112.
- Pratt B. R. (2001) Oceanography, bathymetry and syndepositional tectonics of a Precambrian intracratonic basin: integrating sediments, storms, earthquakes and tsunamis in the Belt Supergroup (Helena Formation, ca. 1.45 Ga), western North America. *Sed. Geol.* **141–142**, 371–394.
- Qi H., Coplen T. B., Geilmann H., Brand W. A. and Böhlke J. K. (2003) Two new organic reference materials for $\delta^{13}\text{C}$ and $\delta^{15}\text{N}$ measurements and a new value for the $\delta^{13}\text{C}$ of NBS 22 oil. *Rapid Commun. Mass Spectrom.* **17**, 2483–2487.
- Quan T. M. and Falkowski P. G. (2009) Redox control of N:P ratios in aquatic ecosystems. *Geobiology* **7**, 124–139.
- Rau G. H., Arthur M. A. and Dean W. E. (1987) $15\text{N}/14\text{N}$ variations in Cretaceous Atlantic sedimentary sequences: implications for past changes in marine nitrogen biogeochemistry. *Earth Planet. Sci. Lett.* **82**, 269–279.
- Reinhard C. T., Raiswell R., Scott C. T., Anbar A. and Lyons T. W. (2009) A late Archean sulfidic sea stimulated by early oxidative weathering of the continents. *Science* **326**, 713–716.
- Reinhard C. T., Planavsky N. J., Robbins L. J., Partin C. A., Gill B. C., Lalonde S. V., Bekker A., Konhauser K. O. and Lyons T. W. (2013) Proterozoic ocean redox and biogeochemical stasis. *Proc. Natl. Acad. Sci.* **110**, 5357–5362.
- Rivera K. T., Puckette J. and Quan T. M. (2015) Evaluation of redox versus thermal maturity controls on $\delta^{15}\text{N}$ in organic rich shales: a case study of the Woodford Shale, Anadarko Basin, Oklahoma, USA. *Org. Geochem.* **83**, 127–139.
- Robinson R. S., Kienast M., Albuquerque A. L., Altabet M., Contreras S., De Pol Holz R., Dubois N., Francois R., Galbraith E., Shu T.-C., Ivanochko T., Jaccard S., Kao S.-J., Kiefer T., Kienast S., Lehmann M., Martinez P., McCarthy M., Moebius J., Pedersen T., Quan T. M., Ryabenko E., Schmittner A., Schneider R., Schneider-Mor A., Shigemitsu M., Sinclair D., Somes C., Studer A., Thunell R. and Yang J.-Y. (2012) A review of nitrogen isotopic alteration in marine sediments. *Paleoceanography* **27**. <http://dx.doi.org/10.1029/2012PA002321>.
- Robl T. L. and Davis B. H. (1993) Comparison of the HF-HCl and HF-BF₃ maceration techniques and the chemistry of resultant organic concentrates. *Org. Geochem.* **20**, 249–255.
- Rooze J. and Meilie C. (2016) The effect of redox conditions and bioirrigation on nitrogen isotope fractionation in marine sediments. *Geochim. Cosmochim. Acta* **184**, 227–239.
- Saito M. A., Sigman D. M. and Morel F. M. M. (2003) The bioinorganic chemistry of the ancient ocean: the co-evolution of cyanobacterial metal requirements and biogeochemical cycles at the Archean-Proterozoic boundary? *Inorg. Chim. Acta* **356**, 308–318.
- Schidlowski M. (1987) Application of stable carbon isotopes to early biochemical evolution on Earth. *Annu. Rev. Earth Planet. Sci.* **15**, 47–72.
- Schoepfer S. D., Henderson C. M., Garrison G. H. and Ward P. D. (2012) Cessation of a productive coastal upwelling system in the Panthalassic Ocean at the Permian-Triassic Boundary. *Palaeogeogr. Palaeoclimatol. Palaeoecol.* **313–314**, 181–188.
- Scott C., Wing B. A., Bekker A., Planavsky N. J., Medvedev P., Bates S. M., Yun M. and Lyons T. W. (2014) Pyrite multiple-sulfur isotope evidence for rapid expansion and contraction of the early Paleoproterozoic seawater sulfate reservoir. *Earth Planet. Sci. Lett.* **389**, 95–104.
- Sephton M. A., Amor K., Franchi I. A., Wignall P. B., Newton R. and Zonneveld J.-P. (2002) Carbon and nitrogen isotope disturbances and an end-Norian (Late Triassic) extinction event. *Geology* **30**, 1119–1122.
- Shen Y., Knoll A. H. and Walter M. R. (2003) Evidence for low sulphate and anoxia in a mid-Proterozoic marine basin. *Nature* **423**, 632–635.
- Siebert C., Kramers J. D., Meisel T., Morel P. and Naegler T. F. (2005) PGE, Re-Os, and Mo isotope systematics in Archean and early Proterozoic sedimentary systems as proxies for redox conditions of early Earth. *Geochim. Cosmochim. Acta* **69**, 1787–1801.
- Sigman D. M., Altabet M. A., McCorkle D. C., Francois R. and Fischer G. (2000) The $\delta^{15}\text{N}$ of nitrate in the southern ocean: nitrogen cycling and circulation in the ocean interior. *J. Geophys. Res.: Oceans* **105**, 19599–19614.
- Sigman D. M., DiFiore P. J., Hain M. P., Deutsch C., Wang Y., Karl D. M., Knappe A. N., Lehman M. F. and Pantoja S. (2009a) The dual isotope of deep nitrate as a constraint on the cycle and budget of oceanic fixed nitrogen. *Deep Sea Res. Part I* **56**, 1419–1439.
- Sigman D. M., Karsh K. L. and Casciotti K. L. (2009b) *Ocean process tracers: nitrogen isotopes in the ocean*. *Encyclopedia of ocean science*. Elsevier, Amsterdam, pp. 4138–4153.
- Siljeström S., Volk H., George S. C., Lausmaa J., Sjövall P., Dutkiewicz A. and Hode T. (2013) Analysis of single oil-bearing fluid inclusions in mid-Proterozoic sandstones (Roper Group, Australia). *Geochim. Cosmochim. Acta* **122**, 448–463.
- Sperling E. A., Wolock C. J., Morgan A. S., Gill B. C., Kunzmann M., Halverson G. P., Macdonald F. A., Knoll A. H. and Johnston D. T. (2015) Statistical analysis of iron geochemical data suggests limited late Proterozoic oxygenation. *Nature* **523**, 451–454.
- Stüeken E. E. (2013) A test of the nitrogen-limitation hypothesis for retarded eukaryote radiation: nitrogen isotopes across a Mesoproterozoic basinal profile. *Geochim. Cosmochim. Acta* **120**, 121–139.
- Stüeken E. E., Catling D. C. and Buick R. (2012) Contributions to late Archean sulphur cycling by life on land. *Nat. Geosci.* **5**, 722–725.
- Stüeken E. E., Buick R. and Guy B. M. (2015a) Isotopic evidence for biological nitrogen fixation by Mo-nitrogenase at 3.2 Gyr. *Nature* **520**, 666–669.
- Stüeken E. E., Buick R. and Anbar A. D. (2015b) Selenium isotopes support free O₂ in the latest Archean. *Geology* **43**, 259–262.

- Stüeken E. E., Kipp M. A., Koehler M. C. and Buick R. (2016) The evolution of Earth's biogeochemical nitrogen cycle. *Earth Sci. Rev.* **160**, 220–239.
- Summons R. E., Powell T. G. and Boreham C. J. (1988) Petroleum geology and geochemistry of the Middle Proterozoic McArthur Basin, Northern Australia: III. Composition of extractable hydrocarbons. *Geochim. Cosmochim. Acta* **52**, 1747–1763.
- Symons D. T. A. (1966) A paleomagnetic study on the Gunflint, Mesabi, and Cuyuna iron ranges in the Lake Superior region. *Econ. Geol.* **61**, 1336–1361.
- Thamdrup B., Dalsgaard T. and Revsbech N. P. (2012) Widespread functional anoxia in the oxygen minimum zone of the Eastern South Pacific, Deep-Sea Res. Part I: *Oceanograph. Res. Pap.* **65**, 36–45.
- Tesdal J. E., Galbraith E. D. and Kienast M. (2013) Nitrogen isotopes in bulk marine sediment: linking seafloor observations with subsurface records. *Biogeosciences* **10**, 101–118.
- Thomazo C. and Papineau D. (2013) Biogeochemical cycling of nitrogen on the early Earth. *Elements* **9**, 345–351.
- Thomson D., Rainbird R. H., Planavsky N., Lyons T. W. and Bekker A. (2015) Chemostratigraphy of the Shaler Supergroup, Victoria Island, NW Canada: a record of ocean composition prior to the Cryogenian glaciation. *Precamb. Res.* **263**, 232–245.
- Thunell R. C., Sigman D. M., Muller-Karger F., Astor Y. and Varela R. (2004) Nitrogen isotope dynamics of the Cariaco Basin, Venezuela. *Global Biogeochem. Cycles* **18**. <http://dx.doi.org/10.1029/2003GB002185>.
- Tyrrell T. (1999) The relative influences of nitrogen and phosphorus on oceanic primary production. *Nature* **400**, 525–531.
- Volk H., George S. C., Dutkiewicz A. and Ridley J. (2005) Characterisation of fluid inclusion oil in a Mid-Proterozoic sandstone and dolerite (Roper Superbasin, Australia). *Chem. Geol.* **223**, 109–135.
- Wang X., Shi X., Tang D. and Zhang W. (2013) Nitrogen isotope evidence for redox variations at the Ediacaran-Cambrian transition in South China. *J. Geol.* **121**, 489–502.
- Wille M., Kramers J. D., Naegler T. F., Beukes N. J., Schroeder S., Meisel T., Lacassie J. P. and Voegelin A. R. (2007) Evidence for a gradual rise of oxygen between 2.6 and 2.5 Ga from Mo isotopes and Re-PGE signatures in shales. *Geochim. Cosmochim. Acta* **71**, 2417–2435.
- Wingate M. T. D. (2002) Age and palaeomagnetism of dolerite sills of the Bangemall Supergroup on the Edmund 1:250,000 map sheet, WA. Western Australia Geological Survey Record, 2002/4.
- Winston D. (1990) Evidence for intracratonic, fluvial and lacustrine settings of middle to late Proterozoic basins of western USA. In *Mid-Proterozoic Laurentia-Baltica* (eds. C. F. Gower, T. Rivers and B. Ryan). Geological Association Canada, Special Papers, pp. 535–564.
- Yamaguchi K. E. (2002) *Geochemistry of Archean-Paleoproterozoic Black Shales: The early Evolution of the Atmosphere, Oceans, and Biosphere* (Ph.D. dissertation). Pennsylvania State University, p. 485.
- Zerkle A. L., House C. H., Cox R. P. and Canfield D. E. (2006) Metal limitation of cyanobacterial N₂ fixation and implications for the Precambrian nitrogen cycle. *Geobiology* **4**, 285–297.
- Zerkle A., Junium C. K., Canfield D. E. and House C. H. (2008) Production of ¹⁵N-depleted biomass during cyanobacterial N₂-fixation at high Fe concentrations. *J. Geophys. Res.: Biogeosci.* **113**. <http://dx.doi.org/10.1029/2007JG000651>.
- Zerkle A. L., Claire M. W., Domagal-Goldman S. D., Farquhar J. and Poulton S. W. (2012) A bistable organic-rich atmosphere on the Neoproterozoic Earth. *Nat. Geosci.* **5**, 359–363.
- Zhang X., Sigman D. M., Morel F. M. and Kraepiel A. M. (2014) Nitrogen isotope fractionation by alternative nitrogenases and past ocean anoxia. *Proc. Natl. Acad. Sci.* **111**, 4782–4787.
- Zhang S., Wang X., Wang H., Bjerrum C. J., Hammarlund E. U., Costa M. M., Connelly J. N., Zhang B., Su J. and Canfield D. E. (2016) Sufficient oxygen for animal respiration 1,400 million years ago. *Proc. Natl. Acad. Sci.* **113**, 1731–1736.
- Zi J. W., Rasmussen B., Muhling J. R., Fletcher I. R., Thorne A. M., Johnson S. P., Cutten H. N., Dunkley D. J. and Korhonen F. J. (2015) In situ U-Pb geochronology of xenotime and monazite from the Abra polymetallic deposit in the Capricorn Orogen, Australia: dating hydrothermal mineralization and fluid flow in a long-lived crustal structure. *Precamb. Res.* **260**, 91–112.

Associate editor: James Farquhar